Cancer Letters 529 (2022) 153–167

Contents lists available at ScienceDirect

Cancer Letters

journal homepage: www.elsevier.com/locate/canlet

Original Articles

Inhibition of the endosomal recycling pathway downregulates HER2 activation and overcomes resistance to tyrosine kinase inhibitors in HER2-positive breast cancer

Anurag Mishra, David Hourigan, Andrew J. Lindsay *

Membrane Trafficking and Disease Laboratory, School of Biochemistry & Cell Biology, Biosciences Institute, University College Cork, Cork, T12 YT20, Ireland

ARTICLE INFO

Keywords:
Endosomal recycling pathway
HER2-targeted therapies
Drug synergy
Drug resistance
Primaquine

ABSTRACT

The development of HER2-targeted therapies has led to a dramatic improvement in outcomes for breast cancer patients. However, nearly all patients with metastatic HER2-positive breast cancer will eventually progress on these therapies due to innate or acquired resistance. Recent evidence suggests that the endosomal recycling of HER2 plays an important role in regulating its oncogenic signalling. Here we report that the expression of Rab coupling protein (RCP), a key regulator of endosomal recycling, positively correlates with that of HER2 and HER3 in breast tumours, and high *RCP* expression is predictive of poor relapse-free and overall survival in patients with HER2-amplified breast cancer. Chemical and genetic inhibition of endosomal recycling leads to a reduction in the total cellular levels of HER2 and HER3 and inhibits the activation of their downstream signalling pathways. We find that HER2 and HER3 that have been internalised from the plasma membrane are diverted to lysosomes for degradation when endosomal recycling is blocked. Primaquine (PQ), a small molecule inhibitor of the endosomal recycling pathway, synergises with HER2-targeting tyrosine kinase inhibitors and overcomes innate and acquired resistance to these TKIs. Moreover, TKI-induced drug tolerant persister cells are vulnerable to endosomal recycling inhibitors. These findings suggest that inhibition of endosomal recycling represents a promising therapeutic strategy for treating drug resistant HER2-positive breast cancer.

1. Introduction

Human epidermal growth factor receptor 2 (HER2) is overexpressed in 20–25% of breast cancers worldwide, and is associated with aggressive disease and poor survival [1]. This has established HER2 as a therapeutic target and tumour biomarker, and the advent of HER2-targeting therapies has led to a remarkable improvement in the outlook for patients with early stage HER2-positive breast cancer. Nevertheless, a significant proportion of these patients will develop progressive disease and die of breast cancer [2]. Furthermore, 40–50% of women with advanced HER2-positive breast cancer will develop brain metastases during the course of their illness. Novel therapeutic strategies are clearly needed to tackle innate and acquired resistance to HER2-targeted therapies.

HER2 has no known ligand and instead activates downstream signalling pathways by forming heterodimers with other members of the ErbB receptor tyrosine kinase family. HER3 is the preferred dimerization partner for HER2, and the HER2-HER3 heterodimer is the most potent pair of all the ErbB family members in terms of interaction strength and ligand-induced tyrosine phosphorylation. This complex activates several intracellular signalling cascades including cell proliferation and survival pathways [3,4]. Oncogenic signalling and intracellular trafficking of receptor tyrosine kinases (RTKs) is closely coupled in numerous cancers [5]. Cargo internalised from the plasma membrane is delivered to early endosomes where it is sorted for onward transport to distinct cellular destinations. Many cargoes, including RTKs, G-protein coupled receptors, adhesion molecules and immune checkpoint proteins are returned to the cell surface via the endosomal recycling pathway. This pathway is one of the main cellular mechanisms for controlling the composition of the plasma membrane, however it is frequently dysregulated in cancer [6].

The endosomal pathway controls the strength and duration of signalling by many RTKs, including the epidermal growth factor receptor (EGFR), MET and IGF1 receptor. In comparison to these receptors, our

Abbreviations: RCP, Rab coupling protein; RTK, Receptor tyrosine kinase; TKI, Tyrosine kinase inhibitor.

* Corresponding author.
E-mail address: a.lindsay@ucc.ie (A.J. Lindsay).

https://doi.org/10.1016/j.canlet.2022.01.003
Received 6 December 2021; Accepted 3 January 2022
Available online 7 January 2022

understanding of the details of HER2 and HER3 trafficking are limited and contradictory. HER2 localises almost exclusively to the plasma membrane and it has been suggested that endocytosis does not play an important role in its signalling and turnover. This 'limited-internalisation' model proposes that lack of a cognate ligand, the absence of an internalisation motif on its intracellular domain, an inhibitory effect on clathrin-coated pit formation and its association with the Hsp90 chaperone, renders HER2 resistant to endocytosis [7]. An alternative 'rapid recycling' model proposes that the swift return of endocytosed HER2 to the plasma membrane accounts for its almost exclusive localisation at the cell surface [7].

Evidence supporting the 'rapid recycling' model includes the observation that HER2 localises to lipid raft subdomains of the plasma membrane and physically interacts with the lipid-raft associated oncoprotein Mucin 1 (MUC1) [8], and that HER2 is internalised via caveolae, cholesterol- and sphingolipid-enriched invaginations of the plasma membrane [9,10]. Recently, it was reported that sortilin-related receptor 1 (SorLA), a multifunctional intracellular sorting protein, promotes the endosomal recycling of internalised HER2 and HER3 back to the plasma membrane [11,12]. Silencing of SorLA inhibits the recycling of HER2 and triggers its targeting to lysosomes where it is degraded, and sensitizes HER2-overexpressing cells to a lysosome modifying drug [11], and drug-resistant breast cancer cells to the tyrosine-kinase inhibitor (TKI) neratinib [12].

Rab coupling protein (RCP), a key regulator of endosomal recycling, has previously been shown to promote the recycling of EGFR, in complex with α5β1 integrin, to the leading edge of ovarian cancer cells [13]. We reported that RCP regulates the recycling of N-cadherin to the plasma membrane in non-small cell lung cancer (NSCLC) cells and that its downregulation leads to a reduction in total N-cadherin protein levels by diverting the internalised adhesion protein into the degradative pathway [14]. In this study we investigated whether inhibition of the endosomal recycling pathway would similarly downregulate RTK levels and their signalling in HER2-positive breast cancer cells. We report that RCP expression positively correlates with that of HER2 and HER3 in breast cancer cell lines and breast tumours, and we found that chemical and genetic inhibition of endosomal recycling leads to a reduction in the activation and total protein levels of HER2 and HER3. We show that the endosomal recycling inhibitor primaquine (PQ) synergises with HER2-targeting monoclonal antibody and small molecule therapies. This synergy is also found in cells that have developed acquired or innate resistance to lapatinib, an FDA-approved dual EGFR/HER2 tyrosine kinase inhibitor (TKI). We also demonstrate that lapatinib-resistant cells have enhanced sensitivity to PQ, likely due to its ability to cross-inhibit the autophagy pathway. A growing body of evidence has shown that autophagy is a key regulator in the development of resistance to targeted therapies. We conclude that inhibiting the endosomal recycling pathway may be a viable strategy for downregulating clinically relevant cell surface proteins and a novel means of overcoming resistance to targeted therapies.

2. Materials and methods

2.1. Materials

Recombinant HRGβ1 was from PeproTech (Rocky Hill, NJ) and EGF was from Sigma-Aldrich. Primaquine and all cell culture reagents were from Sigma-Aldrich. Lapatinib, neratinib, afatinib and MTT were from Carbosynth, UK. LysoTracker Red DND-99 and DQ-Ovalbumin were from ThermoFisher Scientific, UK.

Antibodies specific for HER2 (Rabbit, #4290), HER3 (Rabbit, #12708), p-Y1221/1222 HER2 (Rabbit, #2243), p-Y1248 HER2 (Rabbit, #2247), p-Y1289 HER3 (Rabbit, #2842), pan-Akt (Mouse, #2920) p-S473 Akt (Rabbit, #9271), Erk 1/2 (Mouse, #4696), p-T202/Y204 Erk 1/2 (Rabbit, #4370), mTor (Rabbit, #2972), p-S2448 mTor (Rabbit, #2971), S6 Ribosomal Protein (Mouse, #2971), and p-S235/236 S6 Ribosomal Protein (Rabbit, #2211) were from Cell Signalling Technology, Danvers, MA. Anti-alpha tubulin (Mouse, T9026) and anti-RCP (Chicken, GW21574A) are from Sigma-Aldrich, anti-p62/SQSTM1 (Mouse, MA5-27800) is from Life Technologies and mouse monoclonal HER2 (3B5) and mouse monoclonal (RTJ.2) are from Santa Cruz. Trastuzumab (FT6504) was purchased from Carbosynth, UK.

2.2. Cell culture

SK-BR-3 and BT474 HER2-overexpressing breast cancer cells (CalTag Medsystems, UK) were cultured in McCoy's 5A modified and Dulbecco's modified Eagle's medium, respectively, supplemented with 10% heat-inactivated foetal bovine serum, 100 U/ml penicillin, 100 μg/ml streptomycin and 2 mM L-glutamine (Sigma). JIMT-1 and MDA-MB-453 were cultured in RPMI supplemented with 10% heat-inactivated foetal bovine serum, 100 U/ml penicillin, 100 μg/ml streptomycin and 2 mM L-glutamine (Sigma). Cells were cultured at 37 °C in a humidified atmosphere at 5% CO_2. BT474 and SK-BR-3 cells with acquired resistance to lapatinib were generated by culturing parental cells with increasing concentrations of lapatinib over the course of 6–9 months. All cells were determined to be free of mycoplasma.

To knockdown RCP or HER2 expression, two independent siRNA duplexes to each gene were obtained (Sigma). A siRNA duplex targeting firefly luciferase was used as a negative control. Reverse transfections were performed with a final siRNA concentration of 20 nM using Lipofectamine RNAiMax (Thermo Fisher), according to the manufacturer's instructions. Cell lysates were prepared 48 h post-transfection.

For growth factor stimulation, BT474 cells were seeded and cultured to 70–80% confluency. They were then incubated in serum-free medium in the presence or absence 10 μM primaquine for 24 h prior to stimulation with 10 ng/ml of growth factor for 10 min. To terminate stimulation, cells were immediately placed on ice and washed with cold PBS. Lysosome function was inhibited by co-treating the cells with 20 mM NH_4Cl for 24 h prior to cell lysis and proteasome activity was inhibited with 1 μM MG132 for 24 h.

For single and combination drug treatments, cells were seeded and cultured to 70–80% confluency. The media was then replaced with fresh complete medium plus lapatinib, PQ or the combination of both, and returned to the incubator for 24 h.

2.3. Bioinformatic analyses

Breast cancer patient survival data were analysed using the Kaplan-Meier Plotter online survival analysis platform (http://kmplot.com) which contains transcriptomic and survival data for 7830 breast cancer samples. When performing the regression analyses, all possible cutoff values between the upper and lower quartiles were determined and the best performing cutoff was used to generate the Kaplan-Meier plots [15].

RCP, HER2, and *ERBB3 (HER3)* gene expression of 57 breast cancer cell lines available in the Cancer Cell Line Encyclopedia (CCLE) were determined and the median gene expression for *HER2*-and *ERBB3*- was used to divide the datasets into high (above median) and low (below median) expressing groups. The same strategy was used to analyse 1923 breast tumours from the METABRIC study that is available on the cBioPortal database [16,17].

The protein levels of RCP, HER2 and HER3 in breast cancer cell lines available in the DepMap Portal database were downloaded and imported into GraphPad Prism where they were subjected to a simple linear regression analysis.

2.4. Immunoblot analysis

Whole-cell lysates were prepared in RIPA buffer supplemented with protease and phosphatase inhibitors. Following incubation on ice, nuclear and cellular debris was removed by centrifugation at 20,000×*g*. Protein concentration was determined by Bradford assay, and samples

were denatured at 95 °C for 5 min in 4X loading buffer. Equal amounts of proteins were resolved by SDS-PAGE and transferred to nitrocellulose. Membranes were reversibly stained with Revert 700 Total Protein Stain (LI-COR Biosciences, UK) and scanned on an Odyssey infrared imaging system (LI-COR Biosciences, UK). The Revert Stain was washed off and the membrane was blocked with Odyssey Blocking Buffer TBS (LI-COR Biosciences, UK) for 1 h at room-temperature. Primary antibodies were diluted in Odyssey Blocking Buffer TBS and incubated with the membranes overnight at 4 °C. IRDye-conjugated secondary antibodies were used for detection with the Odyssey infrared imaging system and densitometry was performed using the Image Studio software from LI-COR. Bands were normalised against the Revert 700 stain for that sample, according to the manufacturer's instructions.

2.5. Cell viability, synergy, clonogenic and 3D spheroid assays

2.5.1. Cell viability

Cell viability was assessed by MTT assay. The HER2-amplified cell lines are slow growing so they were seeded into 96-well plates in 100 μl of growth medium. After 72 h, the cells were exposed to the drugs and drug combinations for a further 72 h. MTT (Carbosynth, UK) was then added for 2–3 h and cells were solubilized in MTT solvent (4 mM HCl, 0.1% NP-40 in isopropanol). The OD_{570} and OD_{630} was measured on a MultiSkan Go plate reader (Thermo Scientific). Quadruplicate wells for each treatment were analysed and each experiment was carried out 3 or more times.

2.5.2. IC_{50} and synergy

The IC_{50} values were determined by nonlinear regression of the dose-response data using GraphPad Prism 9.0 for PC (GraphPad Software, La Jolla, CA). The presence or absence of synergism was determined by the method of Chou and Talalay [18,19]. In brief, cells were exposed to 1:1 ratios of the IC_{50} values of tyrosine kinase inhibitor and PQ at 1/8 x IC_{50}, ¼ x IC_{50}, ½ x IC_{50}, IC_{50}, 2 x IC_{50} and 4 x IC_{50}. Cell viability was determined after 72 h treatment and the CI was calculated using the CompuSyn software [20], to determine the presence of synergism ($CI < 1$) or antagonism ($CI > 1$).

2.5.3. Clonogenic assay

Drug sensitivity was assessed using colony formation/clonogenic assays. 5×10^4 cells were seeded into each well of a 12-well plate and 72 h later the medium was replaced with fresh medium containing the indicated drug and incubated for 10 days. The medium was replaced every 3–4 days. The cells were washed and stained with 0.5% crystal violet in 20% methanol. Plates were scanned on a flatbed scanner and colonies were quantified in ImageJ.

2.5.4. 3D spheroids

BT474 cells readily form spheroids in U-bottomed 96-well suspension plates (Greiner bio-one; #650-185). 5×10^3 cells were seeded in 100 μl growth medium into each well and the plate was centrifuged at 400×*g* for 5 min. The cells were incubated at 37 °C for 48 h to allow the spheroids to form. Drugs were then added and the plate was returned to the incubator for 5 days. For quantitative analysis of spheroid viability resazurin (Sigma-Aldrich) was added to a final concentration of 4.4×10^{-5} M and incubated overnight. Fluorescence (Ex 544/Em 590) was measured on a Flex Station II fluorimeter (Molecular Devices).

The live/dead assay was performed by culturing the spheroids with 2 μM calcein AM (ThermoFisher) and 6 μM ethidium bromide (Sigma-Aldrich) for the final 4 h of the drug treatment. The live spheroids were imaged on a Leica DMI3000 B inverted fluorescence microscope and fluorescence intensity along a line drawn through the centre of each spheroid was quantified using the Plot Profile plugin in ImageJ.

2.5.5. Senescence assays

BT474 cells were seeded at 2.5×10^4 cells per well in a 12-well plate. 24 h later the medium was replaced with fresh medium containing the indicated drugs and cultured for 14 days. The medium was replaced every 3–4 days. SA-βgal activity was detected using the chromogenic method described previously [21]. Multiple fields for each condition were acquired using a Leica DMI3000 B inverted microscope and blue cells displaying SA-βgal activity were counted using the Cell Counter plugin in ImageJ.

2.6. Cell motility assays

2.6.1. Wound healing assay

JIMT-1 cells were seeded in 24-well plates and 72–96 h later, when they had reached confluence, a single line was scratched through the centre of each well with a yellow-tip. The cells were washed with PBS and serum-free media containing 20 ng/ml HRGβ1 plus or minus the indicated concentration of PQ was added to each well. Images were acquired at 4X on a Leica DMI3000 B inverted microscope for the 0-h timepoint. The plate was returned to 37 °C for 18 h and images were acquired again. The distance the cells migrated was determined using ImageJ.

2.6.2. Migration and invasion assays

For the migration assays 10×10^4 JIMT-1 cells in serum-free RPMI plus or minus 50 μM PQ were added to the upper chamber of a Transwell chamber containing 8 μm pores (Corning #3422). Serum-free RPMI plus or minus 20 ng/ml HRGβ1 was added to the lower chamber and the cells were allowed to migrate for 18 h at 37 °C. Cells that had migrated through the membrane and were attached to the underside of the Transwell were fixed and stained with 0.05% crystal violet. Migrated cells were imaged on a brightfield microscope and counted. The invasion assays were performed as above except the Transwell upper chambers were coated with 100 μl of 0.8 mg/ml Matrigel (Corning).

2.7. Fluorescence microscopy

2.7.1. Lysosome analysis

5×10^4 BT474 cells were seeded in 24-well plates on 10 mm glass coverslips and cultured at 37 °C for 48–72 h. The culture medium was replaced with 0.5 ml fresh medium plus drugs and incubated for a further 24 h. For lysosome acidity analysis, the cells were incubated for the final hour with LysoTracker Red, to a final concentration of 75 nM. To measure the activity of the degradative pathway, the cells were incubated with 50 μg/ml DQ-ovalbumin in the presence of the drugs for the final 18 h. Cells were washed with warm PBS and fixed with 4% paraformaldehyde for 15 min at room-temperature and quenched with 50 mM ammonium chloride. Nuclei were labelled with DAPI and the coverslips were mounted on glass slides with MOWIOL.

2.7.2. Colocalization studies

For immunofluorescence microscopy 5×10^4 JIMT-1 cells were seeded in 24-well plates on 10 mm glass coverslips and cultured at 37 °C for 48–72 h. Cells that were treated with growth factor were cultured in serum-free medium overnight prior to stimulation 20 ng/ml HRGβ1 for the indicated times. Complete growth media was used for PQ treatment. After treatment cells were washed with warm PBS and fixed with 4% paraformaldehyde for 15 min at room-temperature and quenched with 50 mM ammonium chloride followed by blocking and permeabilization with 0.05% saponin/0.2% BSA in PBS for approximately 30 min at RT. The coverslips were then transferred to a humid chamber and incubated with the indicated primary antibodies in the blocking solution for 1 h at RT. The secondary antibodies used were Cy3-conjugated donkey anti-rabbit from Jackson ImmunoResearch Laboratories (West Grove, PA) and Alexa^{488}-conjugated goat anti-mouse from Thermo Fisher. The cells were washed extensively with PBS between antibody incubations, and the coverslips were mounted in Mowiol. DAPI was included with the secondary antibodies to label the nuclei.

2.7.3. Image-based endosomal recycling assay

For the endosomal recycling assay, 100 × 10^4 BT-474 cells were seeded in 24-well plates on 10 mm glass coverslips and cultured at 37 °C for 48 h. The media was replaced with fresh media containing 10 μg/ml trastuzumab (Carbosynth, UK) and the antibody-bound HER2 was allowed to internalise overnight at 37 °C. The following day surface-bound antibody was removed by a 2-min acid wash (0.2 M glacial acetic acid, 0.5 M NaCl, pH2.5) followed by two washes with PBS. Internalised HER2 was allowed to undergo recycling for 60 min in complete DMEM medium. The cells were then fixed with 4% PFA and trastuzumab was labelled with $Alexa^{488}$-conjugated donkey anti-human (ThermoFisher). Three randomly chosen fields were acquired per condition with identical microscope settings and the surface and intracellular fluorescence intensities of 5–10 cells per field were measured using ImageJ v1.53. Results are pooled from two independent biological experiments.

2.7.4. Confocal microscopy

Images were acquired with a Zeiss LSM 510 confocal microscope (Carl Zeiss, Jena). 3–4 fields, each containing between 10 and 20 cells, were imaged per condition, per experiment. Fields were randomly chosen using the DAPI filter. All confocal settings were the same for each condition. Regions of interest were manually drawn around each cell using the ROI Manager in ImageJ and fluorescence intensity (LysoTracker Red), organelle number and size (DQ-ovalbumin) or Pearson's colocalization coefficient were quantified using the Zeiss Zen image analysis software. Between 40 and 70 cells were analysed per condition in each experiment for the LysoTracker Red and DQ-Ova experiments, and 15 to 27 cells per condition were analysed for the quantitative colocalization.

2.8. Data analysis

Statistical significance was determined using the Student's *t*-test, or where specified a 1-way analysis of variance, using GraphPad Prism. Significance was classified as a *P*-value of * <0.05, ** <0.01, *** <0.001.

3. Results

3.1. High RCP expression is associated with poor outcome in patients with HER2-positive breast cancer

Given that the *RCP* gene is altered in approximately 15% of breast tumours, with the most frequent alteration being gene amplification (Fig. S1a), we sought to determine if there was a correlation between RCP expression and outcome in breast cancer patients. We stratified breast tumours into those that express high and low levels of RCP using the KM plotter survival analysis tool [15] and were surprised to find that there was no correlation between RCP expression and relapse-free survival when all breast cancers were analysed together (Fig. 1a). Indeed, high RCP expression seemed to slightly improve overall survival (Fig. 1b). However, when we analysed HER2-amplified tumours alone, high *RCP* expression predicts poor relapse-free and overall survival (Fig. 1c and d). We next examined RCP protein expression in various breast cancer cell lines and observed that cell lines that expressed HER2 and/or HER3 possessed the highest levels of RCP (Fig. 2a). Interestingly, the lowest levels of RCP were found in the triple-negative BT549 and MDA-MB-231 cells despite these cell lines expressing the highest levels of EGFR. The non-malignant MCF10A cell line also expressed barely detectable levels RCP protein. To further investigate the correlation between RCP and HER2/HER3 expression we stratified 57 breast cancer cell lines from the Cancer Cell Line Encyclopedia (CCLE) into two groups based on their levels of HER2 or HER3 mRNA [22]. We observed significantly higher *RCP* mRNA expression in the high *HER2*-and *HER3*-expressing groups (Fig. 2b and c), with the strongest correlation between *RCP* and *HER3* (Fig. 2c). This positive correlation between *HER3* and *RCP* expression in cancer cell lines was also observed in almost 2000 breast tumours whose genomic and transcriptomic profiles were analysed by the METABRIC study (Fig. 2d) [23]. To determine if

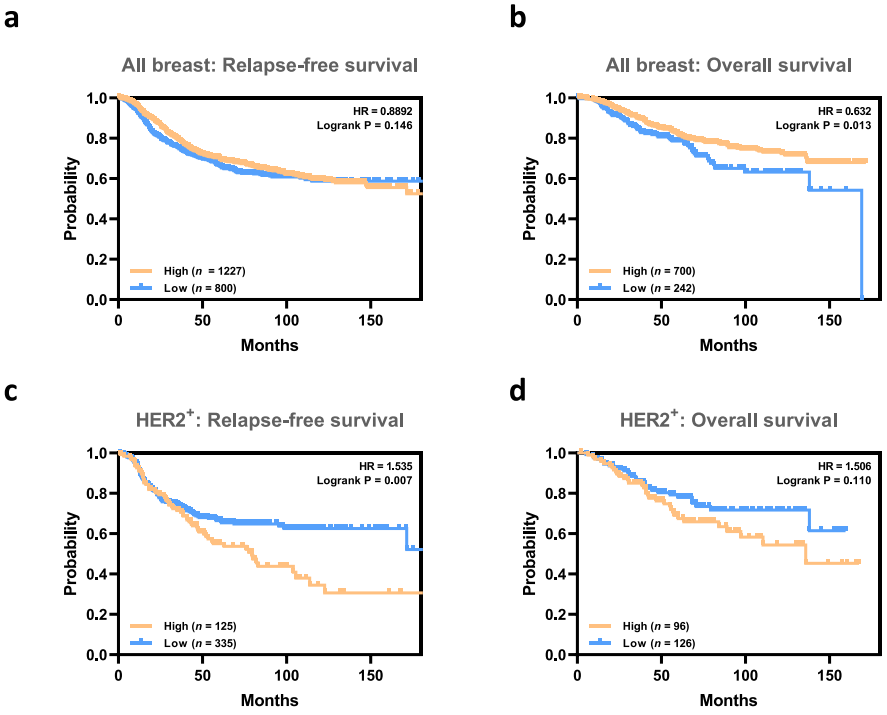

Fig. 1. High RCP expression predicts poor outcome in HER2-positive breast cancer. Kaplan-Meier analysis (http://kmplot.com) of the prognostic value of high versus low RCP mRNA expression (split by best cutoff) for relapse-free survival and overall survival within all breast cancers (**a** and **b**) and HER2-amplified breast cancers (**c** and **d**).

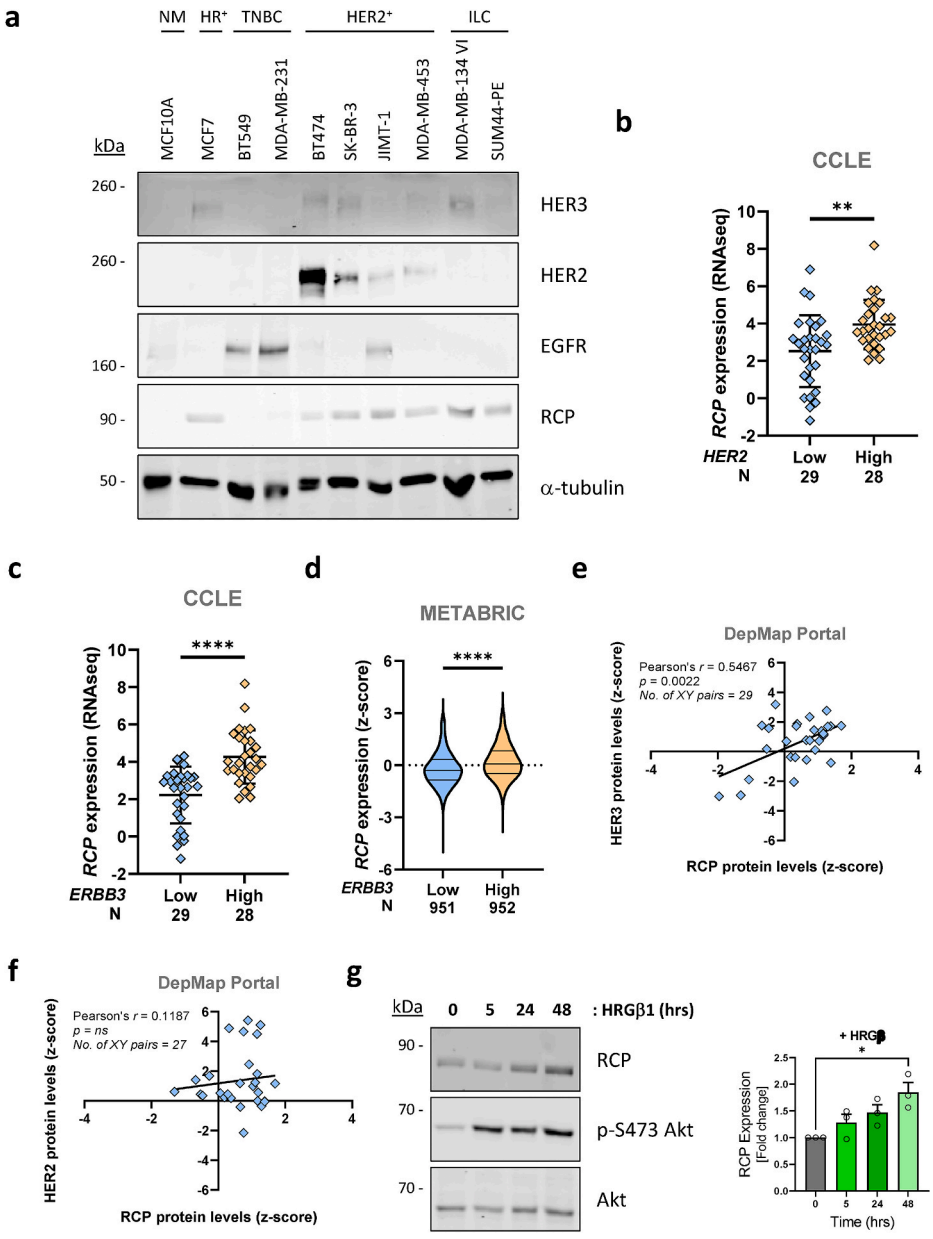

Fig. 2. RCP expression correlates with HER2 and HER3 expression. **a** Western blot analysis of RCP, HER2, HER3 and EGFR protein expression levels in lysates of the indicated breast cancer cell lines. NM non-malignant, $HER2^+$ HER2 amplified, HR^+ hormone receptor positive, TNBC triple-negative breast cancer, ILC invasive lobular carcinoma. **b** *RCP* expression positively correlates with *HER2* expression in breast cancer cell lines from the Cancer Cell Line Encyclopedia ($N = 57$). Data equals mean ± std dev. A Mann-Whitney U statistical analysis test was performed (**$p < 0.01$). **c** *RCP* expression positively correlates with *ERBB3 (HER3)* expression in breast cancer cell lines from the Cancer Cell Line Encyclopedia ($N = 57$). Data equals mean ± std dev. A Mann-Whitney U statistical analysis was performed (****$p < 0.0001$). **d** *RCP* expression positively correlates with *ERBB3* expression in breast tumours analysed by the METABRIC study and accessible in cBioPortal ($N = 1923$). The violin plot depicts the median and 25th and 75th percentiles and the whiskers extend to the maximum and minimum values. Data equals mean ± std dev. A Mann-Whitney U statistical analysis test was performed (****$p < 0.0001$). **e** Proteomic analysis of RCP and HER3 protein levels of breast cancer cell lines available in the DepMap Portal database ($N = 29$). **f** Proteomic analysis of RCP and HER2 protein levels of breast cancer cell lines available in the DepMap Portal database ($N = 29$). **g** BT474 cells were stimulated with 20 ng/ml HRGβ1 for the indicated times. Lysates were made and immunoblotted with the indicated antibodies. The histogram represents the fold difference in RCP protein levels at each time point relative to unstimulated cells.

these correlations also occurred at the protein level, we used the DepMap Portal database to perform a quantitative proteomics analysis of 29 breast cancer cell lines from the CCLE collection [24]. There was strong correlation between RCP and HER3 protein levels (Fig. 2e), but the correlation between RCP and HER2 was weaker (Fig. 2f). To determine if HER2/HER3 heterodimer activation influences the expression of RCP we stimulated BT474 cells with the HER3 ligand heregulin (HRGβ1) for various times over the course of 48 h. A striking increase in RCP protein levels was observed from 24 h of treatment (Fig. 2g). Taken together, these findings reveal that RCP expression is positively regulated by HER2/HER3 in breast cancer.

3.2. RCP colocalises with HER2 and HER3 on intracellular vesicles

BT474 and SK-BR-3 cells express high levels of HER2 (Fig. 2a), however the majority of HER2 in these cell lines is present on the plasma membrane which makes it difficult to visualise an intracellular pool. JIMT-1 and MDA-MB-453 cells express intermediate levels of HER2 and intracellular receptor is easier to distinguish in these cell lines. Therefore, to determine if RCP colocalises with HER2 and HER3 we examined the subcellular distribution of these proteins in serum-starved JIMT-1 cells stimulated with HRGβ1. In control, unstimulated JIMT-1 cells HER2 is present on both the plasma membrane and intracellular vesicles, approximately 13% of which overlapped with RCP (Fig. 3a). In JIMT-1 cells stimulated with HRGβ1 for 1 h, colocalization increased by a factor of 1.7 and HER2 was sometimes observed inside large endosomal structures whose membrane was decorated with RCP (Fig. 3a inset). The colocalization returned to basal levels at 3 h of stimulation. While the colocalization between RCP and HER3 was lower overall (due to the lower amount of HER3 expressed in these cells), the increase in colocalization after 1 h of HRGβ1-stimulation and return to basal levels after 3 h was similar to the HER2 findings (Fig. 3b).

3.3. Inhibiting the endosomal recycling pathway diverts ErbB family members to the degradative pathway

We previously reported that RNAi-mediated knockdown of RCP results in a reduction in the total protein levels of N-cadherin, and

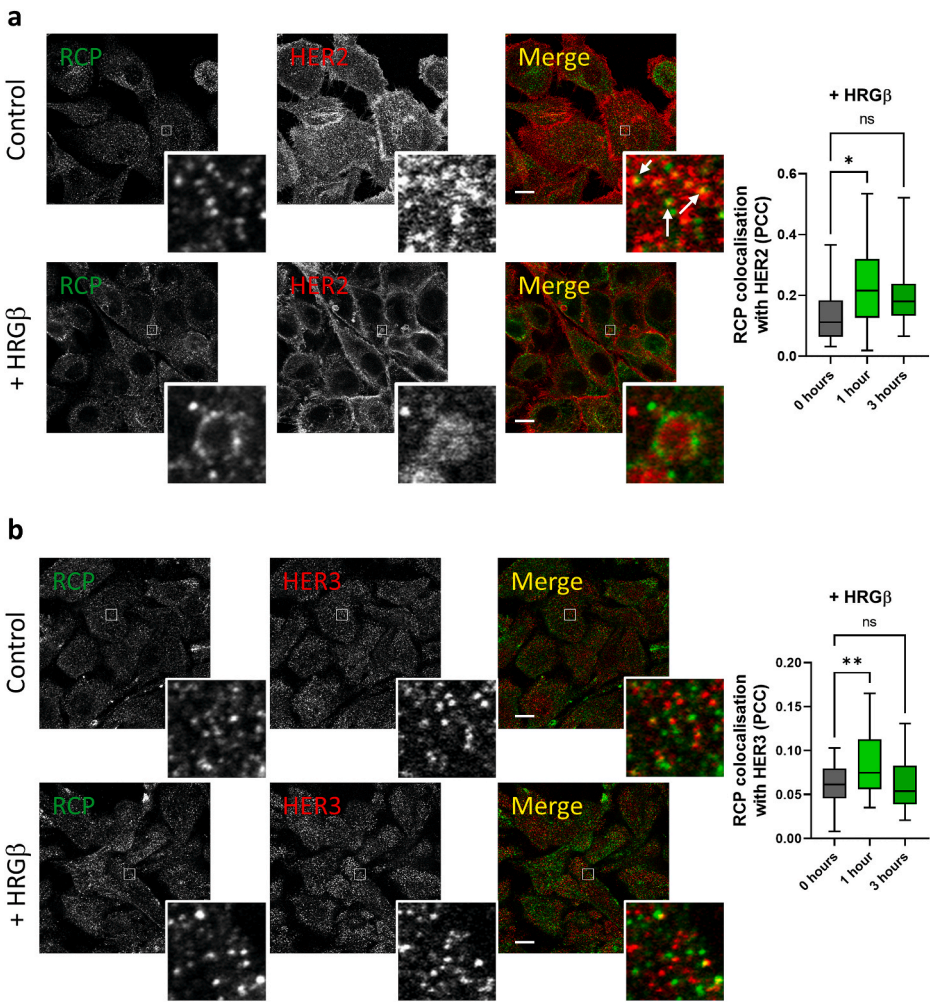

Fig. 3. HRGβ1 induces internalisation and colocalization of HER2 and HER3 with RCP. **a** Representative images of serum-starved JIMT-1 HER2^{+} cells stimulated with 20 ng/ml HRGβ1 for the indicated times prior to fixation and labelling with anti-RCP (green) and anti-HER2 (red). **b** Representative images of serum-starved JIMT-1 HER2^{+} cells stimulated with 20 ng/ml HRGβ1 for the indicated times prior to fixation and labelling with anti-RCP (green) and anti-HER3 (red). The colocalization between RCP and HER2 or HER3 was quantified by determining their Pearson's correlation coefficient (PCC) displayed in the box and whisker plots to the right, which depict the median, 25th and 75th percentiles with the whiskers extending to the maximum and minimum values. Between 15 and 27 cells were analysed per condition (*$p < 0.05$, **$p < 0.01$) from two biological replicates. Bar, 10 μm.

demonstrated that this was due to endocytosed N-cadherin being diverted to lysosomes for degradation [14]. To investigate if this approach could also downregulate HER2 and HER3, RCP was silenced in BT474 cells and the total protein levels of members of the ErbB family of receptor tyrosine kinases was quantified. Greater than 40% reduction in the protein levels of HER3 using two different RCP targeting siRNA duplexes was observed, but there was no effect on HER2 protein levels (Fig. 4a). This suggested that inhibition of the endosomal recycling pathway may be an effective approach for supressing the activity of certain cell surface receptors implicated in cancer. Indeed, silencing of RCP reduced the HRGβ1-induced proliferation of SK-BR-3 cells (Fig. 4b).

We next set out to determine if these findings could be replicated with small molecule inhibitors of endosomal recycling. PQ is a potent inhibitor of trafficking from recycling endosomes to the plasma membrane [25]. Cell viability assays revealed that the HER2 overexpressing cell lines (BT474, SK-BR-3, JIMT-1 and MDA-MB-453) tended to be more sensitive to PQ when compared to other breast and lung cancer cell lines (Table 1). An image-based endosomal recycling assay confirmed

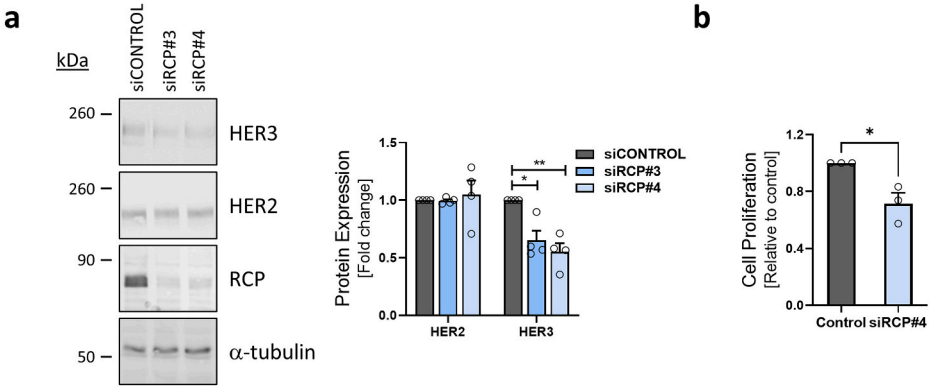

Fig. 4. Depletion of RCP downregulates HER3. **a** Lysates of BT474 cells depleted of RCP were immunoblotted with the indicated antibodies. The histogram represents the fold difference in protein levels relative to cells transfected with a non-targeting siRNA duplex. **b** SK-BR-3 cells were transfected with control non-targeting or RCP-targeting siRNA duplexes and cell proliferation was monitored 5 days post-transfection.

Table 1
IC50 values for primaquine in the indicated cell lines.

Cell line	Primaquine (μmol/L)
BT-474	11.8 ± 1.8
SK-BR-3	4.3 ± 1.1
JIMT-1	20.6 ± 7.5
MDA-MB-453	8.9 ± 0.7
MCF7	21.7 ± 2.1
MDA-MB-231	46 ± 6
SUM44-PE	152.5 ± 28
MDA-MB-134VI	49.1 ± 7.1
MCF10A	32.2 ± 1.3
A549	175 ± 2.8
A431	105 ± 7.3

that PQ inhibits the recycling of internalised HER2. Cell surface HER2 was labelled with trastuzumab and the antibody-bound receptor was endocytosed overnight to saturate the intracellular pool of HER2. Surface-bound trastuzumab was removed with an acid wash and receptor recycling was allowed to occur for 60 min prior to cell fixation and labelling with a fluorescently labelled anti-human antibody. There was a significantly greater pool of intracellular antibody-bound HER2 in the PQ-treated cells, indicating impaired recycling. The majority of trastuzumab-bound HER2 in the control cells was localised to the cell surface (Fig. 5a).

Treatment of BT474 cells with 10 μM PQ for 24 h in serum-free medium resulted in a 50% reduction in HER3 total protein levels (Fig. 5b). Surprisingly, we also observed an ~30% reduction in HER2 levels. The mRNA levels of HER2 and HER3 were not significantly altered by PQ-treatment indicating that the effect of PQ on these receptors was posttranslational (Fig. 5c).

To determine if the PQ-induced degradation of HER2 and HER3 occurred in lysosomes or was mediated by proteasomes, BT474 cells were co-treated with PQ and either the lysosomal inhibitor ammonium chloride or the proteasomal inhibitor MG132. Ammonium chloride restored the levels of HER3 but not HER2, whereas MG132 did not restore the levels of either receptor (Fig. 5d), suggesting that blockade of endosomal recycling results in the diversion of HER3 from the endosomal recycling pathway into the degradative pathway. Interestingly, MG132 on its own also downregulated HER2 and HER3 expression. Proteasomal inhibitors including MG132 have previously been reported to downregulate the expression of ERBB family members and promote their lysosomal degradation [26].

We also observed that PQ induced a 2-fold reduction in the colocalization between HER2 and RCP in JIMT-1 cells (Fig. S2a), while concomitantly increasing HER2 colocalization with the late endosomal protein Rab7 by 3-fold (Fig. S2b).

RCP is a member of the Rab11-FIP family, which is comprised of five members that all play a role in endosomal recycling [27]. It is possible that the differences between RCP silencing and PQ-treatment on the levels of HER2 is due to PQ being a global inhibitor of endosomal recycling whereas each FIP family member regulates a spatially and temporally distinct domain of the endosomal recycling pathway [28],

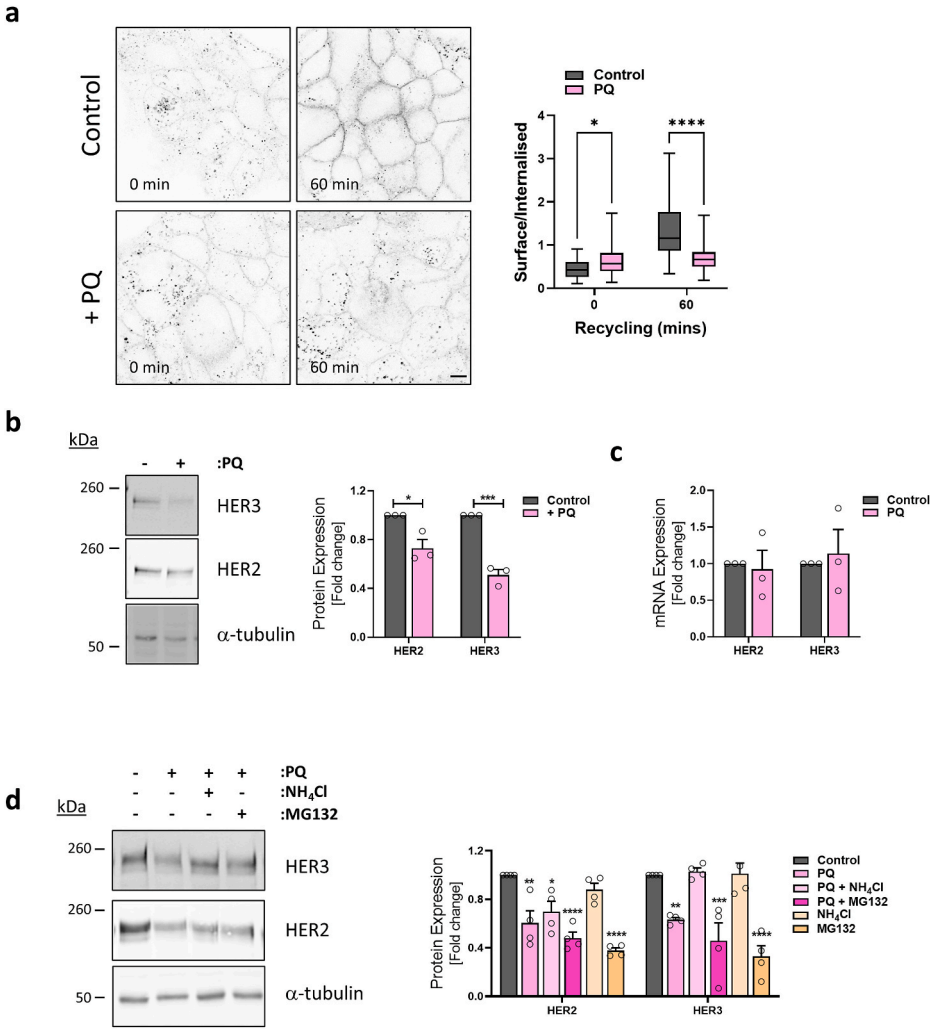

Fig. 5. Inhibition of the endosomal recycling pathway diverts HER2 and HER3 into lysosomes for degradation. **a** HER2 recycling assay in control or PQ-treated BT474 cells. Antibody-bound HER2 was allowed to internalise overnight. Shown are confocal images of cells fixed 0 and 60 min after trastuzumab was stripped from HER2 on the cell surface. The ratio of surface/internalised HER2 is displayed in the box plots (n = 34 Control and 35 PQ-treated cells from two independent experiments; statistical analysis was a two-way ANOVA). **b** BT474 cells were treated with or without 10 μM PQ for 24 h in serum-free medium. Lysates were immunoblotted with the indicated antibodies and the histogram indicates the fold difference in protein levels relative to untreated cells (n = 3). **c** BT474 cells were treated with or without 10 μM PQ for 24 h in serum-free medium and analysed for *HER2* and *HER3* mRNA expression by quantitative real-time, reverse transcriptase PCR (qRT-PCR). The results (mean ± s.e.m. of three biological replicates, each performed in triplicate) are expressed as mRNA expression levels relative to that for control cells. **d** BT474 cells were treated with 10 μM PQ plus or minus 20 mM NH_4Cl or 1 μM MG132 for 24 h in serum-free medium. Lysates were immunoblotted with the indicated antibodies and the histogram indicates the fold difference in protein levels relative to untreated cells (n = 4).

and one of the other FIP family members may regulate the recycling of HER2.

3.4. Primaquine suppresses HER2-mediated signalling

HER2 signalling from the plasma membrane along the PI3 kinase/Akt/mTor and Ras/Raf/MEK/MAPK pathways is critical for the HER2 growth-promoting functions in cancer cells. HER2 has no known ligands and is activated by forming heterodimers with other ErbB family members, including EGFR and HER3 [29]. Serum-starved cells treated with or without PQ for 24 h, were stimulated for 10 min with 10 ng/ml EGF or HRGβ1, the ligands for EGFR and HER3 respectively. Lysates were prepared and analysed for RTK and downstream signalling pathway activation by Western blot. HER2 is constitutively activated in BT474 cells, however PQ suppresses HER2 phosphorylation at tyrosines 1221/1222 and tyrosine 1248 under all conditions (Fig. 6a). HRGβ1 activates HER3, but PQ downregulates the absolute amount of phosphorylated and total HER3 by approximately 2-fold (Fig. 6a). PQ had no effect on mitogen-activated protein kinase (ERK1/2) signalling but inhibited EGF- and HRGβ1-induced Akt-Ser473 phosphorylation (Fig. 6b). No effect was observed on Akt-Thr308 phosphorylation. Akt-Ser473 is a substrate for mammalian target of rapamycin (mTor) [30], so we next investigated the effect of PQ on mTor signalling and observed that it strongly inhibited the activation of mTor and its downstream signalling molecules p70 S6 kinase and S6 ribosomal protein (Fig. 6b). The strong inhibitory effect of PQ on HER2 phosphorylation is likely due to the reduced amount of HER3 available to cross-activate it. Indeed, quantification revealed that while PQ greatly reduces the amount of HER3 in cells, the ratio of activated to total HER3 is unaffected (Fig. S3a). In contrast, there is a greater than 2-fold reduction in the proportion of activated HER2 relative to total HER2 in the PQ-treated cells (Fig. S3b).

Unsurprisingly, we also found that PQ induces a dose-dependent inhibition of HRGβ1-stimulated BT474 cell proliferation. BT474 cells were cultured in the presence of 20 ng/ml HRGβ1 plus increasing concentrations of PQ for 5 days. 2.5 μM PQ led to a 65% inhibition of cell proliferation, whereas there was almost 100% inhibition with 10 μM PQ (Fig. 6c).

HER2-amplified breast cancers are one of the most aggressive subtypes of breast cancer and frequently lead to incurable metastatic disease [31]. To determine if PQ has any effect on the motility of HER2-amplified cells we performed wound healing, migration and invasion assays using JIMT-1 cells. JIMT-1 cells migrate more readily than BT474 and SK-BR-3 cells and we observed that PQ induced a dose-dependent delay in wound closure in 2-dimensional wound healing assays (Fig. S4a). PQ also inhibited the migration and invasion of JIMT-1 cells through extracellular matrix (Figs. S4b and c).

Taken together, these results demonstrate that PQ inhibits the activation of HER2 and HER3 and their downstream PI3 kinase/Akt/mTor signalling pathway leading to a reduction in cell proliferation and motility.

3.5. Primaquine synergises with HER2-targeting tyrosine kinase inhibitors

Since PQ indirectly inhibits HER2 and HER3 activation and downstream signalling by affecting their intracellular trafficking, we next set out to determine whether PQ could enhance the effect of inhibitors that target HER2 directly. Synergy describes an interaction between two or more drugs that results in the total effect of the drugs being greater than the sum of the individual effects of each drug. The use of drug pairs that synergise with each other allows the dosage of the individual drugs to be lowered, thus hopefully reducing toxicity while maintaining the desired clinical effect [32]. Lapatinib (Tykerb®), a reversible dual EGFR/HER2 small molecule TKI, is approved for the treatment of advanced

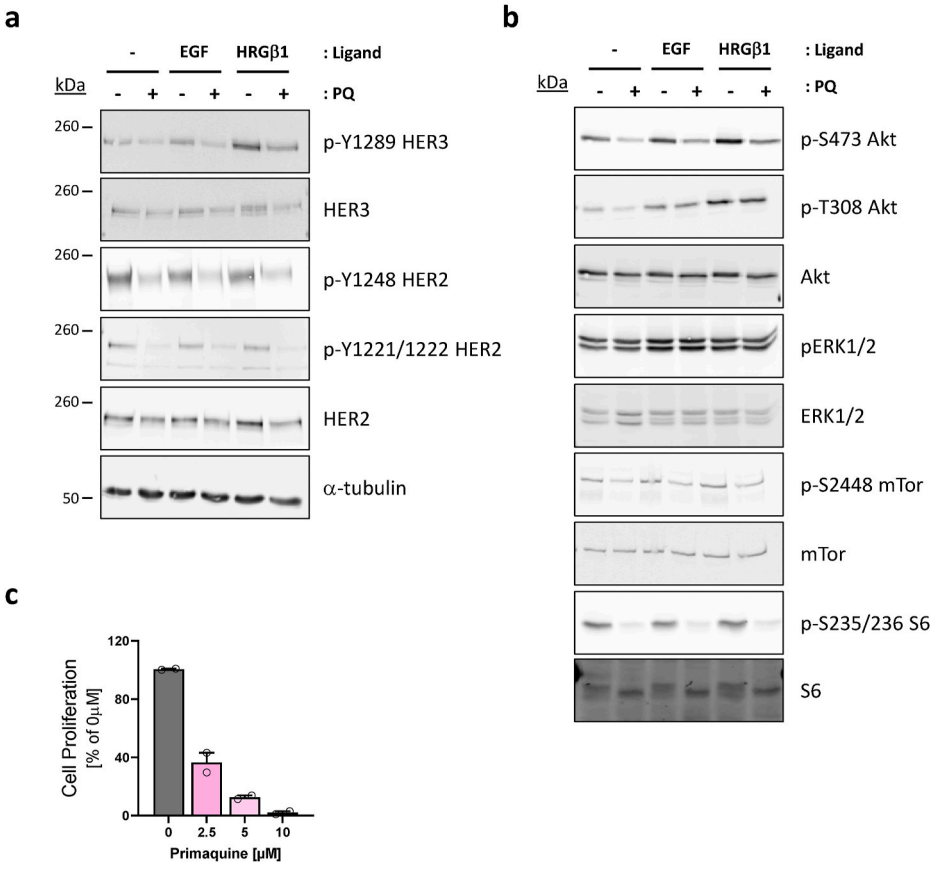

Fig. 6. PQ downregulates ErbB receptor activation and the PI3K/Akt/mTor signalling pathway. **a** and **b** BT474 cells were treated with or without 10 μM PQ for 24 h in serum-free medium and then stimulated with 10 ng/ml EGF or HRGβ1 for 10 min. Lysates were immunoblotted with the indicated antibodies (see Fig. S3 for quantification). **c** BT474 cells seeded the day before in 96-well plates were serum-starved overnight and then stimulated with 20 ng/ml HRGβ1 plus the indicated concentration of PQ for 96 h. Cell proliferation was quantified by MTT assay and expressed as a percentage of control cells not treated with the inhibitor.

HER2-positive breast cancer following progression on previous therapy.

MTT cell viability assays demonstrated decreased cell survival when primaquine and lapatinib were combined (Fig. S5a). Synergy analyses with the CompuSyn software [20,33] indicated that the Combination Index (CI) for lapatinib and PQ was less than 1, suggesting that the relationship between the two drugs is synergistic (Table 2). Strong synergy was also observed between PQ and trastuzumab, a HER2-targeting monoclonal antibody used as a first line treatment for advanced HER2-positive breast cancer (Table 3). Clonogenic assays of BT474 cells treated with sub-lethal doses of lapatinib and PQ (20 nM and 5 μM, respectively) for 10 days revealed an over 10-fold greater inhibition of colony growth for the drug combination when compared to the lapatinib monotherapy (Fig. 7a). Synergy between lapatinib and PQ was also observed by MTT and clonogenic assays in the SK-BR-3 cell line (Figs. S5b and c and Table 2), and in cells grown in 3-dimensional cultures. BT474 cells were cultured in low attachment plates to induce formation of spheroids and were then treated with lapatinib and primaquine, alone or in combination, for 5 days. After the drug treatment the spheroids were exposed to a mixture of calcein AM and ethidium bromide to stain live and dead cells, respectively [34]. Lapatinib alone reduced the growth of the spheroids without affecting the proportion of dead cells, whereas addition of PQ dramatically increased the proportion of dead to live cells (Fig. 7b).

To investigate the effect of the drug combination on HER2 and HER3 activation, lysates of BT474 cells were prepared after a 24-h treatment with 20 nM lapatinib, 10 μM PQ and both drugs combined, in complete serum-containing medium. Western blots revealed that lapatinib induced an upregulation in the total protein levels of HER2 but strongly inhibited its phosphorylation at tyrosines 1221 and 1222. PQ on its own led to a small but significant reduction in HER2 phosphorylation, but the combination of both drugs resulted in the greatest inhibition with an almost 2-fold lower level of phosphorylated HER2 compared to cells treated with lapatinib alone (Fig. 7c). Lapatinib also induced a moderate reduction in the levels of phosphorylated HER3, but this was not enhanced by the addition of PQ (Fig. 7d). Collectively these data demonstrate that the combination of lapatinib and primaquine has a greater inhibitory effect on the activation of HER2 than either drug alone in HER2-overxpressing cells, leading to a reduction in their viability in both 2D and 3D assays.

Table 2
IC50 values for lapatinib, primaquine and their combined effects in the indicated HER2$^+$ cell lines. Drug synergy was assessed by the CI values. CI < 1 = synergy; CI = 1 additivity; CI > 1 = antagonism.

Cell line	Lapatinib (μmol/L)	Primaquine (μmol/L)	Effect (% Death)	Synergy (CI)
BT-474	0.021 ± 0.004		50	
		11.8 ± 1.8	50	
	0.013	1.25	43	0.81
SK-BR-3	0.36 ± 0.09		50	
		4.3 ± 1.1	50	
	0.25	1.25	52	0.54
BT-474 RES	1.15 ± 0.47		50	
		7.7 ± 1.7	50	
	0.5	5	50	0.49
SK-BR-3 RES	5.7 ± 2.2		50	
		13.4 ± 6.2	50	
	5	10	70	0.56
JIMT-1	5.8 ± 2		50	
		20.6 ± 7.5	50	
	5	20	84	0.58
MDA-MB-453	9.2 ± 5.4		50	
		8.9 ± 0.7	50	
	5	5	74	0.52
MCF10A	5.4 ± 0.8		50	
		32.2 ± 1.27	50	
	2.5	12.5	42	1.06

Table 3
IC50 values for trastuzumab, primaquine and their combined effects in BT-474 and BT-474 RES cells. Drug synergy was assessed by the CI values. CI < 1 = synergy; CI = 1 additivity; CI > 1 = antagonism.

Cell line	Trastuzumab (μg/ml)	Primaquine (μmol/L)	Effect (% Death)	Synergy (CI)
BT-474	30.4 ± 1.4		50	
		9.7 ± 0.5	50	
	15	10	82	0.48
BT-474 RES	77.7 ± 3.2		50	
		10.23 ± 0.9	50	
	15	10	59	0.62

3.6. The lapatinib and primaquine combination enhances lysosomal degradation

To gain a greater mechanistic understanding of how the two drugs synergise, we analysed the degradative pathway in BT474 cells treated with lapatinib and primaquine. The lysosome populations in cells treated with the drugs and drug combinations were labelled with LysoTracker Red DND-99, a fluorescent dye that is highly selective for acidic organelles and commonly used to investigate lysosome biogenesis and function. LysoTracker Red was added to the medium for the final hour of drug treatment and the cells were subsequently fixed and analysed by confocal microscopy. A dramatic increase in the size and fluorescence intensity of the lysosome population was observed in cells treated with the drug combination. This phenotype was not observed in cells treated with each drug individually or untreated control cells. Quantitation revealed a 3.4–5.3-fold increase in LysoTracker Red fluorescence intensity (Fig. 8a). Next, we assessed whether the population of lysosomes in the treated cells is functional. To do this we analysed the proteolysis of ovalbumin, a fluid phase marker of late endosomes/lysosomes. DQ-Ova is a self-quenched conjugate of ovalbumin that exhibits bright green fluorescence upon proteolytic degradation [35]. BT474 cells were treated for 24 h with the individual drugs or the combination in the presence of DQ-Ova, followed by fixation and confocal analysis. Quantitation revealed that the drug combination induced a 2.7-fold increase in the number of DQ-Ova positive structures compared to the vehicle control (Fig. 8b). Collectively, these results demonstrate that the combination of lapatinib and PQ results in a dramatic increase in the number and activity of acidic late endosomes/lysosomes. This enhanced activity of the degradative pathway was not observed in cells treated with either drug individually.

3.7. Lapatinib-induced senescent cells are sensitive to primaquine

An augmented lysosomal compartment is a characteristic of cells entering senescence [36]. Cellular senescence is a key component of aging and is induced by stimuli such as DNA damage, telomere shortening and cellular stress. Oncogene signalling can also induce cells to enter senescence, acting as a tumour suppressive mechanism that can prevent or delay malignant progression. Recently therapy-induced senescence (TIS) has been described, where in response to therapy a subpopulation of tumour cells enter a dormant state. TIS can also lead to an alteration of the tumour microenvironment as the senescent cancer cells develop a senescence-associated secretory phenotype (SASP) and release bioactive molecules that can modify the surrounding tumour stroma. The dormant cells may also contribute to the development of resistance by serving as a reservoir of drug resistant cells if their senescent state is reversed [37]. Senescent cells arise continuously in advanced HER2-positive breast cancer and account for approximately 5% of tumour cells in this subtype [38], and recent studies have reported that in addition to inducing apoptosis, lapatinib can also induce senescence [39–41]. Cellular senescence is a slow process which generally requires at least 7 days to develop [42], but it is possible that PQ accelerates the lapatinib-induced entry of HER2-positive cells into a

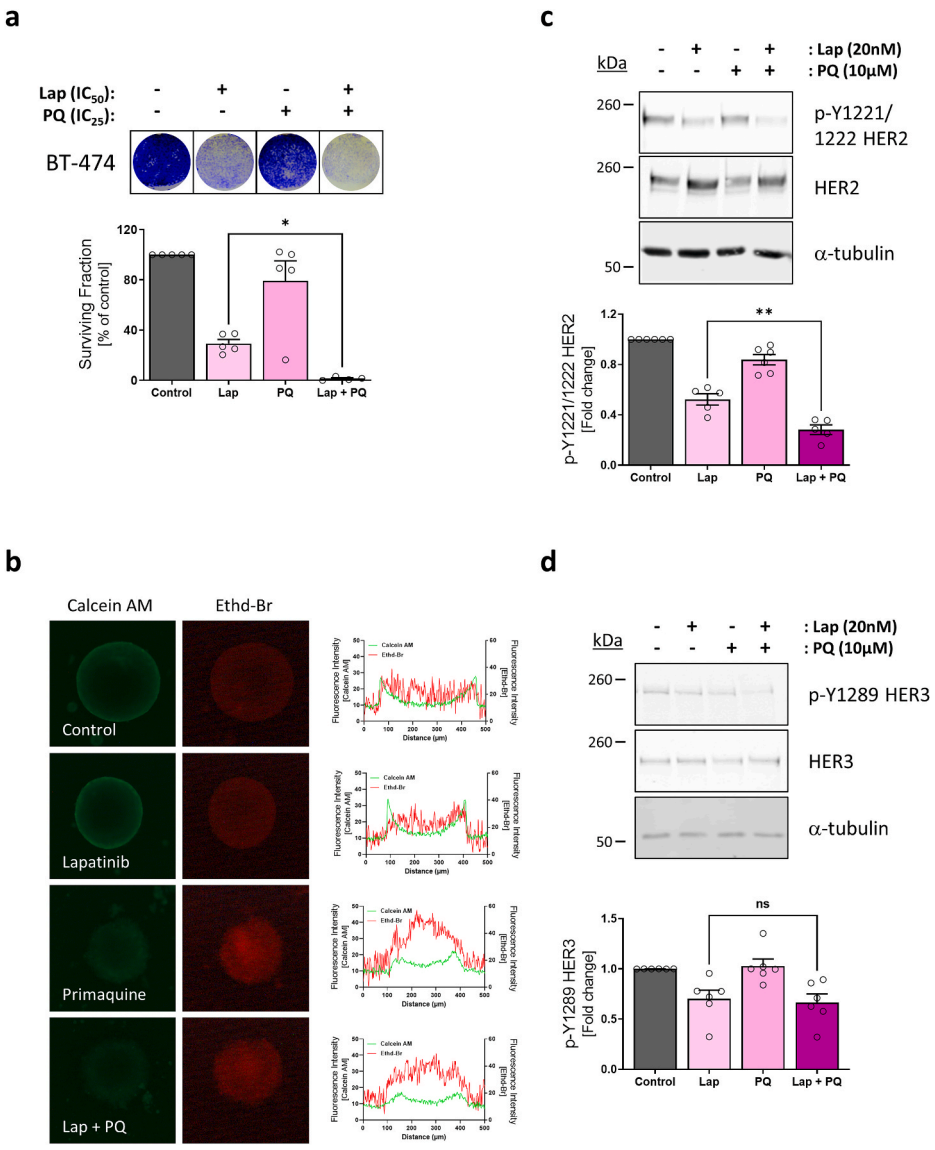

Fig. 7. Primaquine synergises with the HER2-targeting tyrosine kinase inhibitor lapatinib. **a** Clonogenic assays of BT474 cells individually or dual treated with 20 nM lapatinib and 5 μM PQ for 10 days. Histogram indicates the surviving cells expressed as a percentage of the untreated control ($n = 5$). **b** BT474 spheroids treated with 10 nM lapatinib, 5 μM PQ or the combination for 5 days were labelled with Calcein AM (green) and ethidium bromide (red) to label the live and dead cells, respectively. Fluorescence microscopy images of the live spheroids were recorded. The line plots depict the fluorescence intensity profiles along a line through the equator of the spheroids for both channels under each condition. **c** Immunoblots of lysates prepared from BT474 cells treated with lapatinib and PQ for 24 h. The histogram indicates the fold difference in p-Y1221/1222 HER2 phosphorylation levels in the treated cells relative to control cells ($n = 6$). **d** Immunoblots of lysates prepared from BT474 cells treated with lapatinib and PQ for 24 h. The histogram indicates the fold difference in p-Y1289 HER3 phosphorylation levels in the treated cells relative to control cells ($n = 6$).

senescent phenotype. To investigate the ability of primaquine and lapatinib to induce senescence, BT474 cells were treated with each drug individually, or in combination, for 14 days and assessed for senescence-associated beta-galactosidase activity (SA-βgal), a widely used indicator of cellular senescence [21]. As expected, long-term exposure to lapatinib resulted in a 2.6-fold greater number of senescent cells compared to control cells (7.5% in control cells versus 19.3% in the TKI-treated cells), whereas PQ did not induce senescence (Fig. 8c). Interestingly, there were too few viable cells remaining after the combination treatment to accurately quantify SA-βgal activity. A possible explanation for this is that senescent cells are more sensitive to endosomal recycling inhibitors, thus when lapatinib drives cells into senescence they are rapidly killed by the PQ.

To examine this in more detail, we induced senescence in BT474 cells by treating them for 7 days with IC50 and IC90 concentrations of lapatinib. The cells were then treated with 2.5 μM or 5 μM PQ for a further 3 days and cell viability was measured by MTT assay. Control DMSO-treated cells showed no reduction in viability after treatment with either concentration of PQ, whereas 2.5 μM PQ killed virtually all the cells pre-treated with the higher concentration of lapatinib, and 5 μM PQ killed over 70% of the cells pre-treated with the lower dose (Fig. 8d). These findings support the hypothesis that lapatinib-induced senescent cells are sensitised to PQ-induced cell death.

We next investigated why senescent cells are more sensitive to PQ. Evidence is emerging that autophagy, a lysosome-dependent cellular mechanism for removing unnecessary or dysfunctional components, promotes cellular senescence by facilitating the synthesis of senescence associated secretory proteins. To determine if PQ affects autophagy we examined markers of autophagy in drug-treated BT474 cells. PQ induced an increase in the level of the non-lipidated form of LC3B, an indication of reduced autophagic flux (Fig. 8e). Depletion of RCP also induced a similar increase in LC3B levels (Fig. S5d). We also examined the effect of lapatinib and PQ on the levels of p62/SQSTM1 (hereafter p62). p62 interacts with autophagic substrates and delivers them to autophagosomes for degradation and in the process is degraded itself. Thus, induction of autophagy leads to a decrease in p62. We observed that after only 24 h of lapatinib treatment the level of p62 was reduced by approximately 25%, whereas PQ induced a 2-fold increase in p62 levels (Fig. 8f). These findings establish that PQ can inhibit autophagy, and since senescent cells have a greater dependency on this pathway they are likely to be vulnerable to this PQ-induced inhibition of autophagic flux.

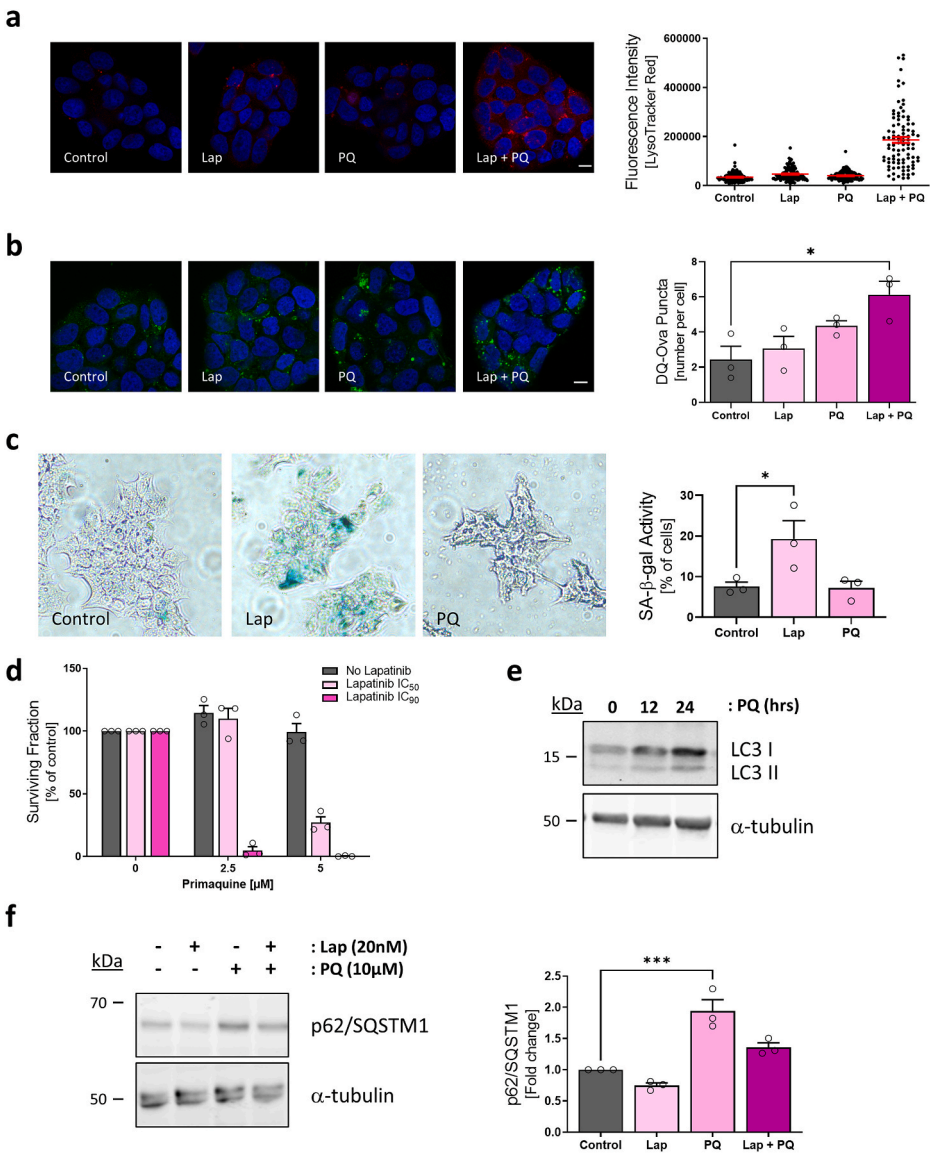

Fig. 8. The lapatinib and primaquine combination upregulates the degradative pathway and blocks autophagic flux. **a** Confocal fluorescence images of BT474 cells treated with the indicated drugs and labelled with LysoTracker Red DND-99 (red). Nuclei are stained with DAPI (blue). Bar, 10 μm. Scatter plot depicts the LysoTracker Red fluorescence intensity of individual cells from each condition. **b** Confocal fluorescence images of BT474 cells treated with the indicated drugs and allowed to internalise DQ-ovalbumin for 18 h. Nuclei are stained with DAPI (blue). Bar, 10 μm. Histogram depicts the mean number of puncta per cell (±s.e.m.). **c** BT474 cells were treated twice weekly with 50 nM lapatinib or 1 μM PQ for a total of 2 weeks and fixed and stained for SA-βgal activity and compared to untreated controls. The histogram indicates the percentage of senescent cells. Error bars indicate the standard error of the means ($n = 3$). **d** BT474 cells were treated with 20 nM (IC_{50}) or 100 nM (IC_{90}) lapatinib for 7 days followed by removal of the TKI and a 3-day treatment with the indicated concentration of PQ. Viable cells were determined by MTT assay. The histogram depicts the surviving cells as a fraction of control cells not treated with PQ ($n = 3$). **e** Immunoblots of lysates prepared from BT474 cells treated with PQ for 0, 12 or 24 h and probed with an antibody to LC3B. **f** Immunoblots of lysates prepared from BT474 cells treated with lapatinib and PQ for 24 h. The histogram indicates the fold difference in p62 levels in the treated cells relative to control cells ($n = 3$).

3.8. *Lapatinib-resistant cells have enhanced sensitivity to primaquine*

Resistance to HER2-targeted therapies is a significant clinical problem. Given the potential therapeutic benefit of the lapatinib/PQ combination, we next investigated whether PQ could be used to overcome acquired and innate resistance to lapatinib. To that end, we generated BT474 and SK-BR-3 cell lines with acquired resistance to lapatinib, by exposing them to increasing concentrations of the TKI over 6–9 months. The resulting BT474-RES cell line had a lapatinib IC_{50} of 1.15 μM, greater than 40 times that of the parental cell line (Fig. 9a, Table 2), and the SK-BR-3 RES cell line had an ~16-fold higher IC_{50} value (Table 2). The BT474-RES cell line is also cross-resistant to trastuzumab (Table 3) and afatinib, a second generation HER2-targeting TKI (Fig. S6d). The resistant cells still respond to lapatinib, as demonstrated by the reduction in pY1221/1222 phosphorylation (Fig. S6a), however they have lost their addiction to HER2 since they can still proliferate when HER2 has been silenced, whereas the parental cells cannot (Figs. S6b and c). In 2-dimensional clonogenic and 3D spheroid assays, the BT474-RES cells were 4.3- and 2- fold more sensitive to PQ than the parental cell line (Fig. 9b and c). Furthermore, the synergy between lapatinib and PQ was consistently stronger in the cell lines with acquired resistance, indicating that the drug combination would be most effective in drug-resistant HER2-positive breast cancer (Fig. 9d and Table 2). Strong synergy was also observed in JIMT-1 and MDA-MB-453 HER2-amplified cell lines which both have innate resistance to lapatinib [43] (Fig. 9d, S7a-d and Table 2). Surprisingly, we observed that treatment with either lapatinib or PQ on their own promoted a 2 to 3-fold increase in proliferation of the JIMT-1 cells, whereas the combination induced a 3-fold reduction in surviving cells compared to the control.

Synergy was also observed between PQ and afatinib and neratinib, second and third generation HER2-targeting TKIs, respectively (Table 4). Interestingly, there was no synergy between PQ and BMS754807 or ponatinib, small molecule inhibitors of the IGF1 receptor and FGF receptor, respectively (Table 4). Thus, it appears that synergy with endosomal recycling inhibitors is specific to HER2-taregting TKIs.

4. Discussion

Despite the success of HER2-targeting monoclonal antibodies and small molecule inhibitors at improving clinical outcomes in women with advanced HER2-positive breast cancer, almost all patients will ultimately experience disease progression. Most to the point where the cancer no longer responds to any approved HER2-targeting therapy. To date there is no standard of care treatment for such patients [2], thus

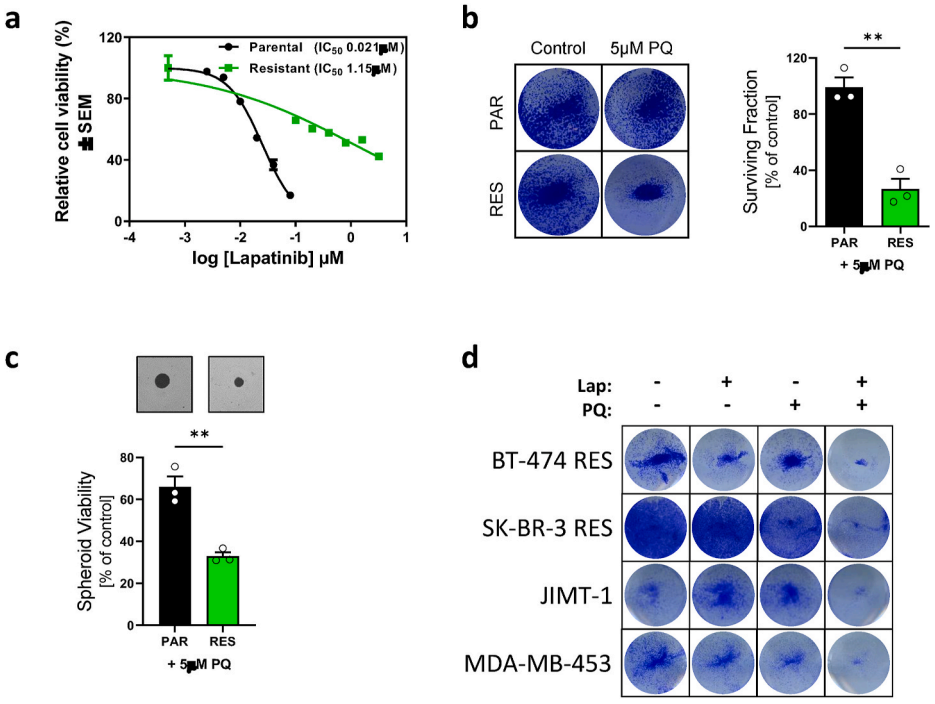

Fig. 9. Lapatinib-resistant HER2-overexpressing breast cancer cells display enhanced sensitivity to primaquine. **a** Cellular viability of BT474 parental (black) and lapatinib-resistant (green) cells treated with lapatinib for 3 days. Data representative of greater than 4 independent experiments. Lapatinib IC_{50} values for both cell lines indicated. **b** Clonogenic assays of parental and lapatinib-resistant BT474 cells treated with 5 μM PQ for 10 days. The histogram indicates the surviving cells expressed as a percentage of the untreated controls. **c** BT474 spheroids treated with 5 μM PQ for 5 days. Spheroid viability was measured by Resazurin assay and expressed as percentage of the viability of untreated parental and resistant spheroids. **d** Representative clonogenic assays of the indicated cell lines individually or dual treated with lapatinib and PQ for 7–14 days (see Fig. S7 for quantification).

Table 4
CI values for PQ in combination with the indicated drugs in BT474 and SK-BR-3 parental and resistant cell lines. CI < 1 = synergy; CI = 1 additivity; CI > 1 = antagonism. ND not done.

CI values	BT474	BT474-RES	SKBR3	SKBR3-RES
Afatinib	0.84 ± 0.04	0.56 ± 0.06	ND	ND
Neratinib	ND	0.54 ± 0.007	0.81 ± 0.07	ND
BMS754807	2.21 ± 0.6	ND	ND	ND
Ponatinib	3.04 ± 0.6	ND	ND	ND

there is a clear unmet need to identify novel therapeutic targets that can be targeted with novel or repurposed agents that can overcome innate and acquired resistance to HER2-targeting therapies.

In many HER2-positive tumours overexpression of HER2 alone is insufficient to drive breast tumour proliferation. Rather, the presence of high levels of HER2 at the plasma membrane promotes the formation of HER2/HER3 heterodimers leading to the activation of HER2 and subsequent HER2-mediated phosphorylation of HER3 [44]. Abrogating the function of HER3 has a similar effect on cell proliferation as directly targeting HER2. Thus, the HER2/HER3 complex functions as an oncogenic subunit that drives HER2-mediated transformation [45]. Due to its lack of intrinsic tyrosine kinase activity HER3 cannot be targeted with TKIs, and of the handful of HER3-targeting therapies at various stages of development none have yet been approved by the FDA [46].

In comparison to EGFR, little is known about the endosomal trafficking of HER2 and HER3. In fact, the predominant hypothesis is that HER2 localises almost exclusively to the plasma membrane and that it resists internalisation, or that any HER2 that is internalised is rapidly recycled back to the plasma membrane [7]. Recently however, the type 1 transmembrane sorting receptor SorLA has been reported to promote the recycling of both internalised HER2 and HER3 back to the plasma membrane [11,12]. Silencing of SorLA targets both receptors to lysosomes for degradation. Here, we report a similar function for the endosomal recycling regulator RCP. We find that downregulation of the endosomal recycling pathway by knockdown of RCP, or treatment with a small molecule inhibitor of endosomal recycling, inhibits the activation of HER2 and its downstream PI3 kinase/Akt/mTor signalling pathway, and ultimately results in the degradation of HER2 and HER3 receptors. The levels of HER3 can be restored by co-treatment with a lysosomal inhibitor, indicating that HER3 is diverted to lysosomes. Our results provide further evidence that similar to other RTKs, HER2 and HER3 undergo endosomal recycling. Together, our findings suggest that inhibition of the endosomal recycling pathway is a means of indirectly targeting these proteins ultimately leading to their downregulation. The observation that lysosomal inhibitors could not restore HER2 protein levels suggest that its turnover may be slower than HER3, which is in line with our findings (not shown) and that of other groups [9].

Given the effect of PQ on the levels and activation of HER2 and HER3, we reasoned that this small molecule might synergise with HER2-targeting therapies. Drug synergy is an interaction between two or more drugs in which the total effect of the drugs in combination is greater than the sum of their individual effect. Synergy can maximise the therapeutic effect of drug combinations while minimizing the adverse effects, because lower doses of the two drugs can be used [47]. Indeed, we found that PQ synergises with lapatinib in six different HER2-amplified cell lines. Furthermore, the synergy was greatest in cell lines with acquired or innate resistance to lapatinib. PQ also synergises with trastuzumab and second and third generation HER2-targeting TKIs. 2D and 3D assays demonstrated that dual treatment with lapatinib and PQ results in greatly enhanced inhibition of the growth and clonogenic survival of both lapatinib –sensitive and –resistant breast cancer cells. Furthermore, drug-resistant BT474 cells display an approximately 2-fold greater sensitivity to PQ, suggesting that resistant cells have enhanced sensitivity to endosomal recycling inhibitors. Our findings (summarized in the model in Fig. 10) indicate that inhibiting the endosomal recycling pathway downregulates HER2 signalling by diverting internalised HER2, and its binding partner HER3, from the recycling pathway and into the degradative pathway. This results in less of the heterodimer at the cell surface and consequently less activation of the PI3 kinase/Akt/mTor pathway.

Additionally, the impact of PQ on cell survival is likely to be enhanced by its inhibitory effect on autophagy. Our discovery that PQ inhibits autophagic flux is unsurprising given that autophagosomes require recycling endosomes for their formation [48,49]. Autophagosomes are double-membrane vesicles that expand and enclose portions

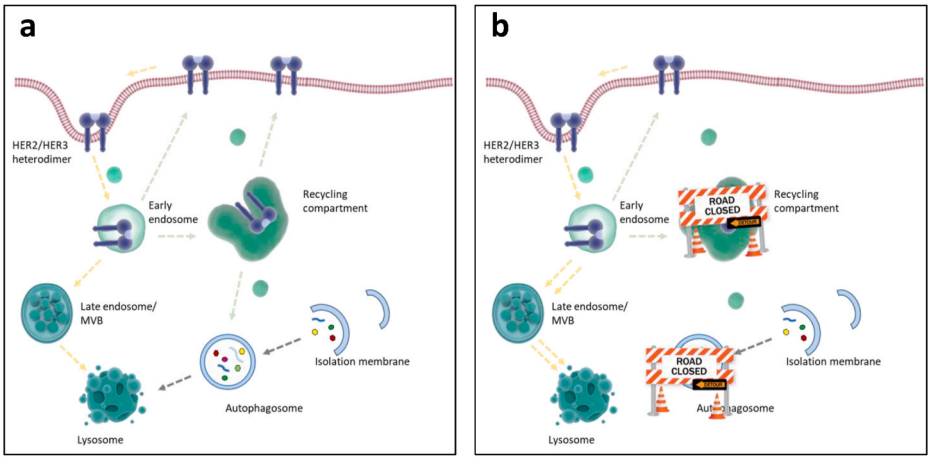

Fig. 10. Schematic depicting the effect of endosomal recycling inhibitors on HER2-amplified breast cancer cells. **a** HER2/HER3 heterodimers are continuously internalised from the plasma membrane and transported to early endosomes. From here they are recycled back to the cell surface, directly or indirectly via the recycling compartment. **b** Small molecule or genetic inhibition of the endosomal recycling pathway simultaneously inhibits autophagic flux and prevents internalised HER2 and HER3 from returning to the plasma membrane, resulting in their diversion to lysosomes for degradation.

of the cytoplasm that contains cellular components destined for autophagic degradation and recycling endosomes have been identified as a platform on which autophagosomes form [50]. Furthermore, inhibition of autophagy disrupts EGFR recycling in multiple cell types [51], and recently autophagy was reported to promote tumorigenesis in HER2-positive breast cancer by blocking the trafficking of HER2 to the plasma membrane [52].

We found that lysosomal acidity and activity is enhanced in cells treated with the lapatinib and PQ combination. An upregulated degradative pathway is a characteristic of senescent cells, and reports are emerging that autophagy and senescence are interdependent [53]. Lapatinib has been reported to induce senescence in HER2-amplified cells [54], and we found that cells exposed to long-term treatment with this TKI have greatly enhanced sensitivity to PQ. We propose that HER2-positive cells that survive the initial lapatinib treatment have been driven into senescence by the TKI, rendering them more vulnerable to the autophagy-inhibitory effects of PQ, ultimately leading to their death. This agrees with recent findings that autophagy promotes the survival of dormant breast cancer cells [55], and that blockade of autophagic flux in genetically engineered mouse models of HER2-positive breast cancer abolishes tumorigenesis [52]. We propose that the cells that resist lapatinib by entering into senescence become dependent on the autophagic pathway, which is in turn downregulated by PQ (Fig. 10b).

Inhibition of the endosomal recycling pathway has also been demonstrated to downregulate other clinically relevant cell surface proteins including PD-L1 [56,57], N-cadherin [14], c-Met [58], integrin β1 [59] and EGFR [13]. Thus, developing therapeutics that target this pathway could have significant clinical benefit, especially for tumours with innate or acquired resistance to targeted therapies [6]. Such drugs are likely to be less susceptible to the emergence of resistance as they indirectly target the cell surface proteins on which they act. PQ is one such inhibitor that has potential therapeutic benefit in cancer. We have shown that it downregulates HER2-mediated growth and clonogenic survival, and since it has been used for decades as an anti-malarial drug it is readily available and has good pharmacokinetic and safety profiles.

In conclusion, we believe that our results and those from other groups demonstrate that the endosomal recycling pathway represents a novel and underexploited target for the development of anti-cancer therapeutics.

Funding

This work was supported by funding from the School of Biochemistry & Cell Biology, UCC.

Author contributions

AM, DH and AJL designed and performed the research. AJL obtained the funding and drafted the manuscript.

Declaration of competing interest

The authors declare that they have no conflicts of interest.

Acknowledgements

We would like to acknowledge Ms Mary O'Sullivan for assistance with cell viability assays and members of the School of Biochemistry & Cell Biology for helpful discussions. Dr Alex Eustace, National Institute for Cellular Biotechnology, Dublin City University kindly provided the JIMT-1 and MDA-MB-453 cell lines.

Appendix A. Supplementary data

Supplementary data to this article can be found online at https://doi.org/10.1016/j.canlet.2022.01.003.

References

[1] C.L. Arteaga, M.X. Sliwkowski, C.K. Osborne, E.A. Perez, F. Puglisi, L. Gianni, Treatment of HER2-positive breast cancer: current status and future perspectives, Nat. Rev. Clin. Oncol. 9 (2012) 16–32, https://doi.org/10.1038/nrclinonc.2011.177.
[2] S. Pernas, S.M. Tolaney, HER2-positive breast cancer: new therapeutic frontiers and overcoming resistance, Ther. Adv. Med. Oncol. 11 (2019), https://doi.org/10.1177/1758835919833519.
[3] R. Pinkas-Kramarski, L. Soussan, H. Waterman, G. Levkowitz, I. Alroy, L. Klapper, S. Lavi, R. Seger, B.J. Ratzkin, M. Sela, Y. Yarden, Diversification of Neu differentiation factor and epidermal growth factor signaling by combinatorial receptor interactions, EMBO J. 15 (1996) 2452–2467, https://doi.org/10.1002/j.1460-2075.1996.tb00603.x.
[4] D. Graus-Porta, R.R. Beerli, J.M. Daly, N.E. Hynes, ErbB-2, the preferred heterodimerization partner of all ErbB receptors, is a mediator of lateral signaling, EMBO J. 16 (1997) 1647–1655, https://doi.org/10.1093/emboj/16.7.1647.
[5] I. Mellman, Y. Yarden, Endocytosis and cancer, Cold Spring Harbor Perspect. Biol. (2013), https://doi.org/10.1101/cshperspect.a016949.
[6] M.J. O'Sullivan, A.J. Lindsay, The endosomal recycling pathway-at the crossroads of the cell, Int. J. Mol. Sci. (2020) 6074, https://doi.org/10.3390/ijms21176074, 2020.
[7] V. Bertelsen, E. Stang, The mysterious ways of ErbB2/HER2 trafficking, Membranes 4 (2014) 424–446, https://doi.org/10.3390/membranes4030424.
[8] D. Raina, Y. Uchida, A. Kharbanda, H. Rajabi, G. Panchamoorthy, C. Jin, S. Kharbanda, M. Scaltriti, J. Baselga, D. Kufe, Targeting the MUC1-C oncoprotein downregulates HER2 activation and abrogates trastuzumab resistance in breast cancer cells, Oncogene 33 (2014) 3422–3431, https://doi.org/10.1038/onc.2013.308.
[9] P.M.R. Pereira, S.K. Sharma, L.M. Carter, K.J. Edwards, J. Pourat, A. Ragupathi, Y. Y. Janjigian, J.C. Durack, J.S. Lewis, Caveolin-1 mediates cellular distribution of

HER2 and affects trastuzumab binding and therapeutic efficacy, Nat. Commun. (2018), https://doi.org/10.1038/s41467-018-07608-w.
[10] M. Sung, X. Tan, B. Lu, J. Golas, C. Hosselet, F. Wang, L. Tylaska, L. King, D. Zhou, R. Dushin, J.S. Myers, E. Rosfjord, J. Lucas, H.P. Gerber, F. Loganzo, Caveolae-mediated endocytosis as a novel mechanism of resistance to trastuzumab emtansine (T-DM1), Mol. Cancer Therapeut. (2018), https://doi.org/10.1158/1535-7163.MCT-17-0403.
[11] M. Pietilä, P. Sahgal, E. Peuhu, N.Z. Jäntti, I. Paatero, E. Närvä, H. Al-Akhrass, J. Lilja, M. Georgiadou, O.M. Andersen, A. Padzik, H. Sihto, H. Joensuu, M. Blomqvist, I. Saarinen, P.J. Boström, P. Taimen, J. Ivaska, SORLA regulates endosomal trafficking and oncogenic fitness of HER2, Nat. Commun. 10 (2019) 1–16, https://doi.org/10.1038/s41467-019-10275-0.
[12] H. Al-Akhrass, J.R.W. Conway, A.S.A. Poulsen, I. Paatero, J. Kaivola, A. Padzik, O. M. Andersen, J. Ivaska, A feed-forward loop between SorLA and HER3 determines heregulin response and neratinib resistance, Oncogene 407 (40) (2021) 1300–1317, https://doi.org/10.1038/s41388-020-01604-5, 2021.
[13] P.T. Caswell, M. Chan, A.J. Lindsay, M.W. McCaffrey, D. Boettiger, J.C. Norman, Rab-coupling protein coordinates recycling of α5β1 integrin and EGFR1 to promote cell migration in 3D microenvironments, J. Cell Biol. 183 (2008) 143–155, https://doi.org/10.1083/jcb.200804140.
[14] A.J. Lindsay, M.W. McCaffrey, Rab coupling protein mediated endosomal recycling of N-cadherin influences cell motility, Oncotarget 8 (2017) 104717–104732, https://doi.org/10.18632/oncotarget.10513.
[15] B. Győrffy, Survival analysis across the entire transcriptome identifies biomarkers with the highest prognostic power in breast cancer, Comput. Struct. Biotechnol. J. 19 (2021) 4101–4109, https://doi.org/10.1016/J.CSBJ.2021.07.014.
[16] E. Cerami, J. Gao, U. Dogrusoz, B.E. Gross, S.O. Sumer, B.A. Aksoy, A. Jacobsen, C. J. Byrne, M.L. Heuer, E. Larsson, Y. Antipin, B. Reva, A.P. Goldberg, C. Sander, N. Schultz, The cBio cancer genomics portal: an open platform for exploring multidimensional cancer genomics data, Cancer Discov. 2 (2012) 401–404, https://doi.org/10.1158/2159-8290.CD-12-0095.
[17] B. Pereira, S.-F. Chin, O.M. Rueda, H.-K.M. Vollan, E. Provenzano, H.A. Bardwell, M. Pugh, L. Jones, R. Russell, S.-J. Sammut, D.W.Y. Tsui, B. Liu, S.-J. Dawson, J. Abraham, H. Northen, J.F. Peden, A. Mukherjee, G. Turashvili, A.R. Green, S. McKinney, A. Oloumi, S. Shah, N. Rosenfeld, L. Murphy, D.R. Bentley, I.O. Ellis, A. Purushotham, S.E. Pinder, A.-L. Børresen-Dale, H.M. Earl, P.D. Pharoah, M. T. Ross, S. Aparicio, C. Caldas, The somatic mutation profiles of 2,433 breast cancers refine their genomic and transcriptomic landscapes, Nat. Commun. 71 (7) (2016) 1–16, https://doi.org/10.1038/ncomms11479, 2016.
[18] T.C. Chou, P. Talalay, Quantitative analysis of dose-effect relationships: the combined effects of multiple drugs or enzyme inhibitors, Adv. Enzym. Regul. 22 (1984) 27–55, https://doi.org/10.1016/0065-2571(84)90007-4.
[19] T.C. Chou, Drug combination studies and their synergy quantification using the chou-talalay method, Cancer Res. 70 (2010) 440–446, https://doi.org/10.1158/0008-5472.CAN-09-1947.
[20] T.C. Chou, N. Martin, CompuSyn for Drug Combinations, A Comput. Softw. Quant. Synerg. Antagon. Determ. IC50, ED50 LD50 Values, [PC Softw. User's Guid. Paramus, NJ, 2005.
[21] F. Debacq-Chainiaux, J.D. Erusalimsky, J. Campisi, O. Toussaint, Protocols to detect senescence-associated beta-galactosidase (SA-βgal) activity, a biomarker of senescent cells in culture and in vivo, Nat. Protoc. 412 (4) (2009) 1798–1806, https://doi.org/10.1038/nprot.2009.191, 2009.
[22] J. Barretina, G. Caponigro, N. Stransky, K. Venkatesan, A.A. Margolin, S. Kim, C. J. Wilson, J. Lehár, G.V. Kryukov, D. Sonkin, A. Reddy, M. Liu, L. Murray, M. F. Berger, J.E. Monahan, P. Morais, J. Meltzer, A. Korejwa, J. Jané-Valbuena, F. A. Mapa, J. Thibault, E. Bric-Furlong, P. Raman, A. Shipway, I.H. Engels, J. Cheng, G.K. Yu, J. Yu, P. Aspesi, M. De Silva, K. Jagtap, M.D. Jones, L. Wang, C. Hatton, E. Palescandolo, S. Gupta, S. Mahan, C. Sougnez, R.C. Onofrio, T. Liefeld, L. MacConaill, W. Winckler, M. Reich, N. Li, J.P. Mesirov, S.B. Gabriel, G. Getz, K. Ardlie, V. Chan, V.E. Myer, B.L. Weber, J. Porter, M. Warmuth, P. Finan, J. L. Harris, M. Meyerson, T.R. Golub, M.P. Morrissey, W.R. Sellers, R. Schlegel, L. A. Garraway, The Cancer Cell Line Encyclopedia enables predictive modelling of anticancer drug sensitivity, Nature 483 (2012) 603–607, https://doi.org/10.1038/nature11003.
[23] C. Curtis, S.P. Shah, S.-F. Chin, G. Turashvili, O.M. Rueda, M.J. Dunning, D. Speed, A.G. Lynch, S. Samarajiwa, Y. Yuan, S. Gräf, G. Ha, G. Haffari, A. Bashashati, R. Russell, S. McKinney, A. Langerød, A. Green, E. Provenzano, G. Wishart, S. Pinder, P. Watson, F. Markowetz, L. Murphy, I. Ellis, A. Purushotham, A.-L. Børresen-Dale, J.D. Brenton, S. Tavaré, C. Caldas, S. Aparicio, The genomic and transcriptomic architecture of 2,000 breast tumours reveals novel subgroups, Nat. 486 (2012) 346–352, https://doi.org/10.1038/nature10983, 2012 4867403.
[24] D.P. Nusinow, J. Szpyt, M. Ghandi, C.M. Rose, E.R. McDonald, M. Kalocsay, J. Jané-Valbuena, E. Gelfand, D.K. Schweppe, M. Jedrychowski, J. Golji, D. A. Porter, T. Rejtar, Y.K. Wang, G.V. Kryukov, F. Stegmeier, B.K. Erickson, L. A. Garraway, W.R. Sellers, S.P. Gygi, Quantitative proteomics of the cancer cell line Encyclopedia, Cell 180 (2020) 387–402, https://doi.org/10.1016/j.cell.2019.12.023, e16.
[25] A.W.M. Van Weert, H.J. Geuze, B. Groothuis, W. Stoorvogel, Primaquine interferes with membrane recycling from endosomes to the plasma membrane through a direct interaction with endosomes which does not involve neutralisation of endosomal pH nor osmotic swelling of endosomes, Eur. J. Cell Biol. 79 (2000) 394–399, https://doi.org/10.1078/0171-9335-00062.
[26] T.K. Huynh, C.-Y. Ho, C.-H. Tsai, C.-K. Wang, Y.-J. Chen, D.-T. Bau, C.-Y. Tu, T.-S. Li, W.-C. Huang, Proteasome inhibitors suppress ErbB family expression through HSP90-mediated lysosomal degradation, Int. J. Mol. Sci. 20 (2019) 4812, https://doi.org/10.3390/IJMS20194812.
[27] C.P. Horgan, M.W. McCaffrey, The dynamic Rab11-FIPs, in: Biochem. Soc. Trans., Portland Press, 2009, pp. 1032–1036, https://doi.org/10.1042/BST0371032.
[28] N.W. Baetz, J.R. Goldenring, Rab11-family interacting proteins define spatially and temporally distinct regions within the dynamic Rab11a-dependent recycling system, Mol. Biol. Cell 24 (2013) 643–658, https://doi.org/10.1091/mbc.E12-09-0659.
[29] M.M. Moasser, The oncogene HER2: its signaling and transforming functions and its role in human cancer pathogenesis, Oncogene 26 (2007) 6469–6487, https://doi.org/10.1038/sj.onc.1210477.
[30] D.D. Sarbassov, D.A. Guertin, S.M. Ali, D.M. Sabatini, Phosphorylation and regulation of Akt/PKB by the rictor-mTOR complex, Science (80-.) 307 (2005) 1098–1101, https://doi.org/10.1126/science.1106148.
[31] A.S. Zimmer, A.E.D. Van Swearingen, C.K. Anders, HER2-positive Breast Cancer Brain Metastasis: A New and Exciting Landscape, Cancer Rep., 2020, p. e1274, https://doi.org/10.1002/CNR2.1274.
[32] T. Pemovska, J.W. Bigenzahn, G. Superti-Furga, Recent advances in combinatorial drug screening and synergy scoring, Curr. Opin. Pharmacol. 42 (2018) 102–110, https://doi.org/10.1016/j.coph.2018.07.008.
[33] T.C. Chou, Theoretical basis, experimental design, and computerized simulation of synergism and antagonism in drug combination studies, Pharmacol. Rev. (2006), https://doi.org/10.1124/pr.58.3.10.
[34] M. Zanoni, F. Piccinini, C. Arienti, A. Zamagni, S. Santi, R. Polico, A. Bevilacqua, A. Tesei, 3D tumor spheroid models for in vitro therapeutic screening: a systematic approach to enhance the biological relevance of data obtained, Sci. Rep. (2016), https://doi.org/10.1038/srep19103.
[35] E. Daro, B. Pulendran, K. Brasel, M. Teepe, D. Pettit, D.H. Lynch, D. Vremec, L. Robb, K. Shortman, H.J. McKenna, C.R. Maliszewski, E. Maraskovsky, Polyethylene glycol-modified GM-CSF expands CD11b high CD11c high but not CD11b low CD11c high murine dendritic cells in vivo: a comparative analysis with Flt3 ligand, J. Immunol. 165 (2000) 49–58, https://doi.org/10.4049/jimmunol.165.1.49.
[36] D.J. Kurz, S. Decary, Y. Hong, J.D. Erusalimsky, Senescence-associated β-galactosidase reflects an increase in lysosomal mass during replicative ageing of human endothelial cells, J. Cell Sci. 113 (2000) 3613–3622, https://doi.org/10.1242/jcs.113.20.3613.
[37] S. Zeng, W.H. Shen, L. Liu, Senescence and cancer, Cancer Transl. Med. 4 (2018) 70, https://doi.org/10.4103/CTM.CTM_22_18.
[38] M.F. Zacarias-Fluck, B. Morancho, R. Vicario, A. Luque Garcia, M. Escorihuela, J. Villanueva, I.T. Rubio, J. Arribas, Effect of cellular senescence on the growth of HER2-positive breast cancers, J. Natl. Cancer Inst. 107 (2015) 20, https://doi.org/10.1093/jnci/djv020.
[39] T. Yu, B.J. Cho, E.J. Choi, J.M. Park, D.H. Kim, I.A. Kim, Radiosensitizing effect of lapatinib in human epidermal growth factor receptor 2-positive breast cancer cells, Oncotarget 7 (2016) 79089–79100, https://doi.org/10.18632/oncotarget.12597.
[40] N.T. Conlon, J.J. Kooijman, S.J.C. van Gerwen, W.R. Mulder, G.J.R. Zaman, I. Diala, L.D. Eli, A.S. Lalani, J. Crown, D.M. Collins, Comparative analysis of drug response and gene profiling of HER2-targeted tyrosine kinase inhibitors, Br. J. Cancer 124 (2021) 1249–1259, https://doi.org/10.1038/s41416-020-01257-x.
[41] M.J. Hangauer, V.S. Viswanathan, M.J. Ryan, D. Bole, J.K. Eaton, A. Matov, J. Galeas, H.D. Dhruv, M.E. Berens, S.L. Schreiber, F. McCormick, M.T. McManus, Drug-tolerant persister cancer cells are vulnerable to GPX4 inhibition, Nature 551 (2017) 247–250, https://doi.org/10.1038/nature24297.
[42] J.E. Purvis, K.W. Karhohs, C. Mock, E. Batchelor, A. Loewer, G. Lahav, p53 dynamics control cell fate, Science (80-.) 336 (2012) 1440–1444, https://doi.org/10.1126/SCIENCE.1218351.
[43] N.A. O'Brien, B.C. Browne, L. Chow, Y. Wang, C. Ginther, J. Arboleda, M.J. Duffy, J. Crown, N. O'Donovan, D.J. Slamon, Activated phosphoinositide 3-kinase/AKT signaling confers resistance to trastuzumab but not lapatinib, Mol. Cancer Therapeut. 9 (2010) 1489–1502, https://doi.org/10.1158/1535-7163.MCT-09-1171.
[44] J. Baselga, S.M. Swain, Novel anticancer targets: revisiting ERBB2 and discovering ERBB3, Nat. Rev. Cancer 9 (2009) 463–475, https://doi.org/10.1038/nrc2656.
[45] T. Holbro, R.R. Beerli, F. Maurer, M. Koziczak, C.F. Barbas, N.E. Hynes, The ErbB2/ErbB3 heterodimer functions as an oncogenic unit: ErbB2 requires ErbB3 to drive breast tumor cell proliferation, Proc. Natl. Acad. Sci. U. S. A. 100 (2003) 8933–8938, https://doi.org/10.1073/pnas.1537685100.
[46] X. Liu, S. Liu, H. Lyu, A.I. Riker, Y. Zhang, B. Liu, Development of effective therapeutics targeting HER3 for cancer treatment, Biol. Proced. Online 21 (2019) 1–10, https://doi.org/10.1186/s12575-019-0093-1.
[47] K.R. Roell, D.M. Reif, A.A. Motsinger-Reif, An introduction to terminology and methodology of chemical synergy—perspectives from across disciplines, Front. Pharmacol. 8 (2017) 158, https://doi.org/10.3389/fphar.2017.00158.
[48] A. Longatti, S.A. Tooze, Recycling endosomes contribute to autophagosome formation, Autophagy 8 (2012) 1682, https://doi.org/10.4161/AUTO.21486.
[49] A. Longatti, C.A. Lamb, M. Razi, S. Yoshimura, F.A. Barr, S.A. Tooze, TBC1D14 regulates autophagosome formation via Rab11- and ULK1-positive recycling endosomes, J. Cell Biol. 197 (2012) 659, https://doi.org/10.1083/JCB.201111079.
[50] C. Puri, M. Vicinanza, A. Ashkenazi, M.J. Gratian, Q. Zhang, C.F. Bento, M. Renna, F.M. Menzies, D.C. Rubinsztein, The RAB11A-positive compartment is a primary platform for autophagosome assembly mediated by WIPI2 recognition of PI3P-RAB11A, Dev. Cell 45 (2018) 114–131, https://doi.org/10.1016/J.DEVCEL.2018.03.008, e8.
[51] J. Fraser, J. Simpson, R. Fontana, C. Kishi-Itakura, N.T. Ktistakis, N. Gammoh, Targeting of early endosomes by autophagy facilitates EGFR recycling and

signalling, EMBO Rep. 20 (2019), e47734, https://doi.org/10.15252/EMBR.201947734.
[52] M. Hao, S.K. Yeo, K. Turner, A. Harold, Y. Yang, X. Zhang, J.L. Guan, Autophagy blockade limits HER2+ breast cancer tumorigenesis by perturbing HER2 trafficking and promoting release via small extracellular vesicles, Dev. Cell 56 (2021) 341–355, https://doi.org/10.1016/j.devcel.2020.12.016, e5.
[53] N.H. Patel, S. Bloukh, E. Alwohosh, A. Alhesa, T. Saleh, D.A. Gewirtz, Autophagy and senescence in cancer therapy, in: Adv. Cancer Res., Adv Cancer Res, 2021, pp. 1–74, https://doi.org/10.1016/bs.acr.2021.01.002.
[54] M.S.J. McDermott, N. Conlon, B.C. Browne, A. Szabo, N.C. Synnott, N.A. O'Brien, M.J. Duffy, J. Crown, N. O'Donovan, HER2-targeted tyrosine kinase inhibitors cause therapy-induced-senescence in breast cancer cells, Cancers 11 (2019) 197, https://doi.org/10.3390/cancers11020197.
[55] L. Vera-Ramirez, S.K. Vodnala, R. Nini, K.W. Hunter, J.E. Green, Autophagy promotes the survival of dormant breast cancer cells and metastatic tumour recurrence, Nat. Commun. 91 (9) (2018) 1–12, https://doi.org/10.1038/s41467-018-04070-6, 2018.
[56] M.L. Burr, C.E. Sparbier, Y.C. Chan, J.C. Williamson, K. Woods, P.A. Beavis, E.Y. N. Lam, M.A. Henderson, C.C. Bell, S. Stolzenburg, O. Gilan, S. Bloor, T. Noori, D. W. Morgens, M.C. Bassik, P.J. Neeson, A. Behren, P.K. Darcy, S.J. Dawson, I. Voskoboinik, J.A. Trapani, J. Cebon, P.J. Lehner, M.A. Dawson, CMTM6 maintains the expression of PD-L1 and regulates anti-Tumour immunity, Nature 549 (2017) 101–105, https://doi.org/10.1038/nature23643.
[57] R. Mezzadra, C. Sun, L.T. Jae, R. Gomez-Eerland, E. De Vries, W. Wu, M.E. W. Logtenberg, M. Slagter, E.A. Rozeman, I. Hofland, A. Broeks, H.M. Horlings, L.F. A. Wessels, C.U. Blank, Y. Xiao, A.J.R. Heck, J. Borst, T.R. Brummelkamp, T.N. M. Schumacher, Identification of CMTM6 and CMTM4 as PD-L1 protein regulators, Nature 549 (2017) 106–110, https://doi.org/10.1038/nature23669.
[58] C.A. Parachoniak, Y. Luo, J.V. Abella, J.H. Keen, M. Park, GGA3 functions as a switch to promote met receptor recycling, essential for sustained ERK and cell migration, Dev. Cell 20 (2011) 751–763, https://doi.org/10.1016/j.devcel.2011.05.007.
[59] E.N. Howe, M.D. Burnette, M.E. Justice, P.M. Schnepp, V. Hedrick, J.W. Clancy, I. H. Guldner, A.T. Lamere, J. Li, U.K. Aryal, C. D'Souza-Schorey, J.J. Zartman, S. Zhang, Rab11b-mediated integrin recycling promotes brain metastatic adaptation and outgrowth, Nat. Commun. 11 (2020), https://doi.org/10.1038/s41467-020-16832-2.